DISCLAIMER NOTICE

THIS DOCUMENT IS BEST QUALITY
PRACTICABLE. THE COPY FURNISHED
TO DDC CONTAINED A SIGNIFICANT
NUMBER OF PAGES WHICH DO NOT
REPRODUCE LEGIBLY.

①

THIS DOCUMENT IS BEST QUALITY PRACTICABLE.
THE COPY FURNISHED TO DDC CONTAINED A
SIGNIFICANT NUMBER OF PAGES WHICH DO NOT
REPRODUCE LEGIBLY.

MODULATION TECHNIQUES FOR DEFEATING

PASSIVE RETICLE-BASED INFRARED SYSTEMS

THESIS

AFIT/GE/EE/77-30   Carl F. Moore
                          Capt   USAF
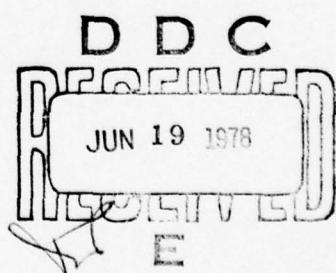
D D C

JUN 19 1978

E

78 06 13 164

MODULATION TECHNIQUES FOR DEFEATING PASSIVE RETICLE-BASED INFRARED SYSTEMS.

Master's thesis,

THESIS

Presented to the Faculty of the School of Engineering

of the Air Force Institute of Technology

Air University

in Partial Fulfillment of the

Requirements for the Degree of

Master of Science

80 p.

by

Carl F. Moore, B.S.

Capt   USAF

Graduate Electrical Engineering

December 1977

Approved for public release; distribution unlimited

012 225

Preface

This thesis was prepared under the sponsorship of the Air Force Avionics Laboratory at Wright-Patterson Air Force Base, Ohio. The purpose of this thesis is to provide a theoretical framework for the study of jamming techniques designed to defeat reticle-based IR systems.

I would like to express my appreciation to my faculty advisor, Captain Stanley R. Robinson, for his guidance and encouragement during this effort. Thanks also go to George Vogel of the Avionics Laboratory for his timely and constructive comments. Finally, special thanks go to my wife, Sharon, for her unfailing support.

Carl F. Moore

Contents

List of Figures

List of Tables

Abstract

A mathematical analysis of an amplitude-modulation (AM), rotating-reticle, infrared (IR) missile system was conducted. Two types of jamming, sinusoidal and noise, were shown to be effective against the AM-reticle system. The following IR modulation techniques which generate these jamming types were discussed: periodic, pseudorandom, and random binary modulation. A method for evaluating the effects of each type of jamming was proposed.

MODULATION TECHNIQUES FOR DEFEATING
PASSIVE RETICLE-BASED INFRARED SYSTEMS

I.   Introduction

One of the most commonly encountered and most consis-
tently effective threats to modern combat aircraft is that
of the infrared (IR) or heat-seeking missile. Recognizing
these facts, the United States Air Force, in general, and
the Air Force Avionics Laboratory, in particular, have spon-
sored a great deal of work on electro-optical (EO) counter-
measures designed to defeat such missiles. This thesis was
undertaken as a part of that effort.

As the title suggests, this thesis investigates the
possibility of using properly modulated IR sources to defeat
or jam infrared missiles. In particular, reticle-based
systems are investigated because they comprise the largest
family of IR systems.

Thesis Limitations

For reasons to be explained later in this report, only
amplitude-modulated (AM), rotating reticle systems will be
analyzed; however, as will also be explained later, it is
hoped that the results for the AM, rotating reticle can be
applied to the jamming of other reticle systems, e.g., fre-
quency-modulated (FM) systems. The analysis in this report

1

will concentrate on the signal processing aspect of an IR system, rather than on the optical or control aspects.

The modulation techniques presented in this report do not represent an exhaustive list. Because of the multitude of possible jamming codes, each of which could introduce new parameters, this report discusses three general types of modulation techniques and presents a method of analyzing each.

Thesis Overview

This thesis begins by briefly reviewing reticle-based IR systems. Next, a mathematical model of how a reticle system turns a spatial scene into an information-bearing electrical signal will be developed. Using such a model, a study will be made of the effects of jamming, both sinusoidal and noise, on the tracking performance of an IR system. Next, a discussion of three types of modulation techniques-- periodic codes, pseudorandom codes, and random binary codes-- will be presented. This report will conclude with a brief summary of the basic findings and with several recommen- dations for future work.

II. Background Material

This chapter will present some of the basic concepts of reticle-based IR systems. For additional information on reticles, the reader is referred to two very readable sources (Ref 1; Ref 2:Ch. 6).

Reticles as Spatial Filters

In IR applications, a reticle, also called a chopper or episcotister, is an optical modulator used to suppress unwanted background signals (a cloud, for example) while enhancing the signals from a target, e.g., a jet engine. This technique of discriminating against objects subtending large angles in favor of objects of small angular extent is called space or spatial filtering.

Figure 1 shows how a reticle fits into a simplified IR tracking system. The field lens focuses the systems' field of view on the reticle. The reticle then chops this radiation by means of a rotating geometrical pattern of transparent and opaque sections. Next, the imaging lens focuses the output field of the reticle onto the entire surface of the optical detector. The entire active area of the detector is illuminated to avoid changes in sensitivity across the surface of the detector. The optical detector converts the radiation incident on its surface into an

electrical signal, the amplitude of which is proportional to the amount of radiation falling on the detector.
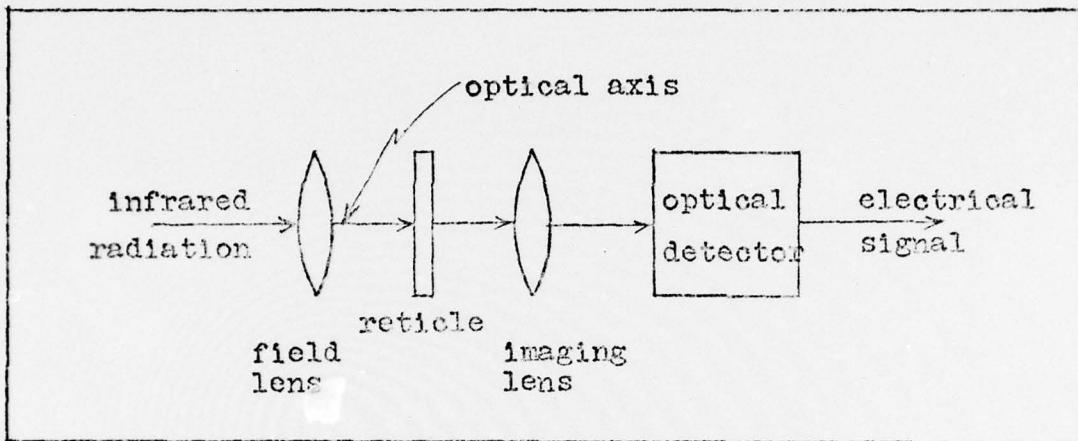
Figure 1. Simple Reticle System

Figure 2 demonstrates the spatial filtering character-istic of a typical reticle. The reticle in this case is fan-shaped with alternating transparent and opaque sections. Imagine the reticle spinning about an axis coincident with the optical axis. Figure 2a shows the detector output for a small point source of light. The radiance from the small source (target) is alternately transmitted and blocked by the rotating sections of the reticle. Thus the output of the detector is periodic with a fundamental frequency, f_c, given by the following expression

$$f_c = nf_r \qquad (1)$$

where n is the number of pairs of clear and opaque sections, and f_r is the rotational frequency of the reticle. Figure 2b

4
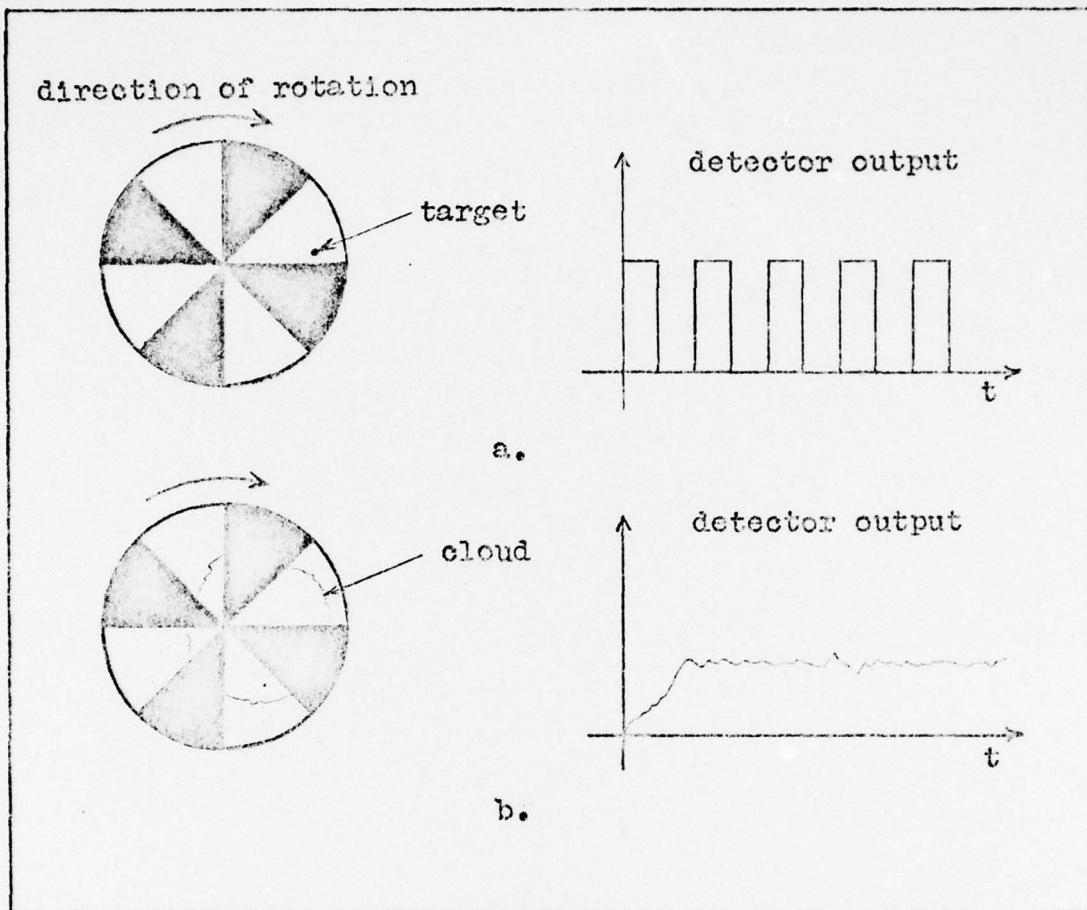
Figure 2. Spatial Filtering Characteristic of a Rotating Reticle

shows the detector output for a large source of infrared
radiation, such as a sunlit cloud. Since the cloud image
covers several segments of the reticle pattern, very little
chopping action is achieved by the reticle. The detector
output, therefore, will be essentially a large constant or
DC value with a small ripple caused by what little chopping
is accomplished.

5

Reticles that Provide Positional Information

The reticle systems under investigation in this paper are used to detect and track particular targets, usually jet airplanes. In these systems it is the function of the reticle to modulate the incident radiance in such a manner as to impart positional information to the detector output. Another important feature of reticle design is that it must provide good background suppression in order to detect targets in the presence of objects with high radiant flux.

The simple two-sector reticle shown in Figure 3 will provide a good example of how reticles provide positional information. Figure 3a shows the detector output when a target is present at position p_1, while Figure 3b depicts the detector output with a target at p_2. The detector output in both cases is a pulse train at the chopping frequency or scan frequency in this case; however, the change in target position from p_1 to p_2 has resulted in a time delay or phase shift in the detector output. Therefore, it is the relative phase angle of the detector output that provides the positional information. Since phase angles must be measured from some reference, a typical phase reference system will consist of a small magnet affixed to the rotating reticle. Each time this magnet passes a small pip coil mounted on the fixed frame of the reticle housing, a sharp pulse is generated which serves as a steady phase reference.

The simple reticle shown in Figure 3 is only capable of producing a phase modulated signal containing the direction

6
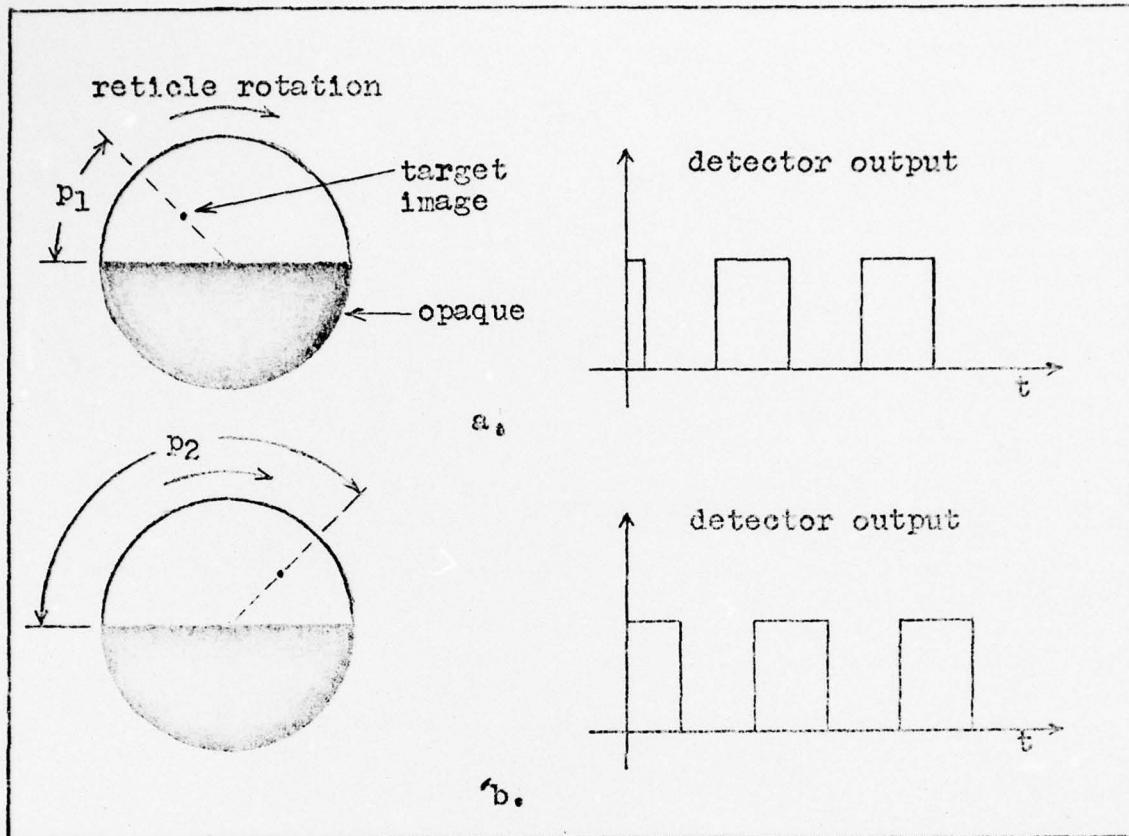
Figure 3. Positional Information Derived from a Simple Two-segment Reticle

of the target from the center of the reticle; it is not capable of determining how far the target is off center nor is it capable of adequate background suppression. Therefore, through judicious use of the 180° transparent section of the simple reticle, these necessary features must be incorporated into the reticle design.

If the 180° transparent segment of the simple reticle is divided into pairs of alternating opaque and transparent, fan-shaped segments, then both requirements can be met. This more complicated reticle is shown in Figure 4. As a target

amplitude-modulating
section

phase-modulating section
(0.5 transmittance)
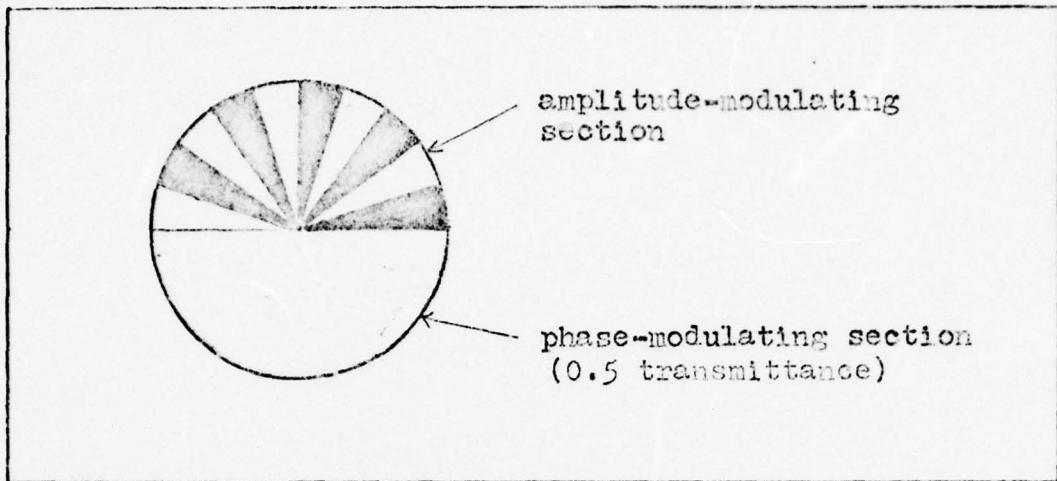
Figure 4. Reticle with Good Background Suppression and Good
Tracking Qualities

image moves radially in or out from the reticle's center,
the detector output is amplitude-modulated. This amplitude-
modulation is caused by the radially changing relationship
between the size of the target image and the size of the fan-
shaped sectors. Thus, the amplitude of the detector output
is directly proportional to the radial position of the target
image.

The fan-shaped segments also help in suppressing back-
ground signals. Early studies on atmospheric background
noise (Ref 1:77-82) determined that substantially no compo-
nent of the detector output due to sky background signals was
found above the eighth harmonic of the reticle scan frequency.
On the other hand, small IR sources, such as jet engines, con-
tributed harmonics out to twenty times the scan rate. Biber-
man and Estey (Ref 1:78-80) patented a reticle that produced

a "carrier" frequency at least eight times higher than the
scan frequency. This reticle cut dramatically the effects
of atmospheric background noise. The carrier frequency of a
reticle system may be computed from the following expression

$$f_c = Knf_r \qquad (2)$$

where f_c is the carrier frequency, K is the reciprocal of
the fraction of the total area of the reticle occupied by
the fan-shaped segments, n is the number of pairs of fan-
shaped sections, and f_r is the rotational frequency of the
reticle. The reticle shown in Figure 4, commonly called a
"rising-sun" reticle, produces a carrier frequency ten times
higher than its scan frequency, and is essentially the reticle
developed by Biberman and Estey.

The phase-modulation portion of the reticle shown in
Figure 4 has a transmittance of 0.5. This is to balance the
radiation through the reticle, and thus suppress a major
background signal at the spin frequency of the reticle.

It is important to note that the relative phase angle
of the carrier does not contain the desired target infor-
mation; rather it is the phase of the envelope of the detec-
tor output that contains the proper positional information.
Figure 5 shows the output of the detector for the reticle of
Figure 4 with the proper phase angle identified.

Reticle Modulation Techniques

Although the reticle shown in Figure 4 produces a signal
that is both phase-modulated and amplitude-modulated, in the

9

detector
output

carrier (10 x scan rate)

t

phase angle containing proper
positional information
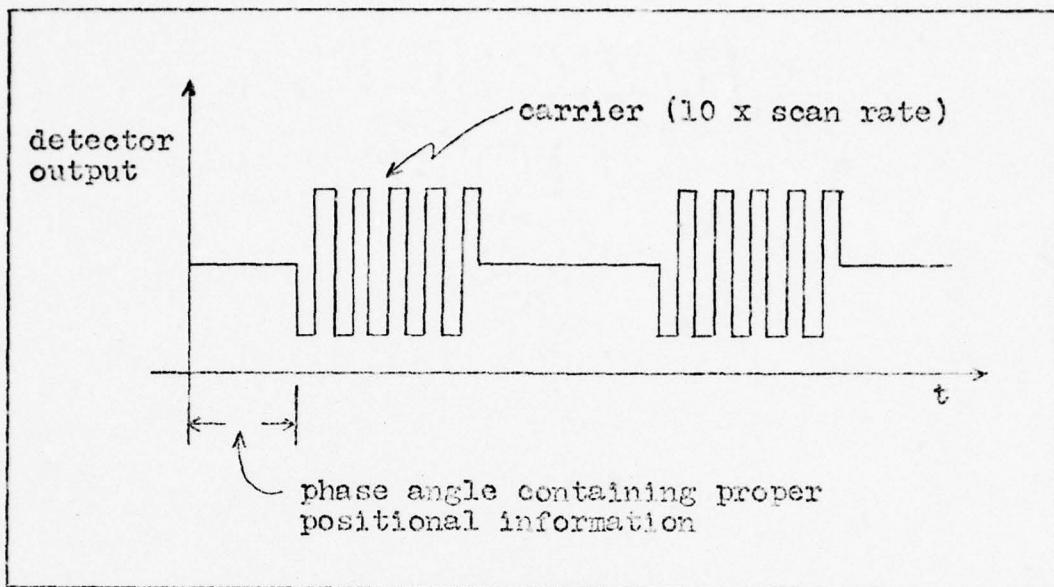
Figure 5. Detector Output from "Rising-Sun" Reticle

nomenclature of reticles it is considered an AM reticle.
This is because reticle systems regularly make use of phase-
modulation for one piece of tracking information, usually
the direction of the target from the reticle center; there-
fore, the modulation technique used to provide the other
piece of tracking information, e.g., distance of target from
reticle center, is commonly used to identify the overall
reticle system. Examples of FM and pulse-duration-modulation
reticle systems are discussed in the literature (Ref 1:34-38;
Ref 2:247-250).

In order to be effective against as many reticle systems
as possible, the analysis in this thesis is directed toward
degrading the phase tracking performance of an IR system.
Thus, the modulation technique needed to provide the other

10

piece of tracking information is of secondary concern. For this reason, the relatively simple AM reticle will suffice as an adequate model for this investigation.

Rotating vs. Stationary Reticles

The discussion thus far has centered around rotating reticles with stationary optics. There is no reason why systems cannot be designed with stationary reticles and rotating optics. Indeed many such systems have been built (Ref 2:250-254). Stationary reticles can offer significant advantages over rotating systems, the most important of which is that there is no loss of carrier for zero pointing error with a stationary reticle.

Since this thesis is a first-cut attempt at applying "smart-jamming" techniques to IR systems, the simpler rotating reticle will serve as a representative model. Again, since both stationary and rotating reticle systems use phase-modulation for directional information, it is anticipated that the results of this report can be extended to stationary reticles as well.

III. Mathematical Analysis of AM-Reticle System

In order to study the effects of jamming on an IR system, a model of how this system processes target information must first be developed. This chapter will analyze the signal-processing portion of a typical AM reticle system and a mathematical model for evaluating jamming techniques will be proposed.

Block Diagram of Typical AM System

Shown in Figure 6 is a block diagram containing the major components of an AM-reticle system. Note that the network after the optical detector is essentially a basic AM detector familiar to electronic communicators.

Optical Detector Output

The output of the optical detector is given by the following expression (Ref 3:1; Ref 4:54; Ref 5:1563)

$$v_a(t) = \int_{-\infty}^{+\infty} \int r(x,y,t)s(x,y,t)dx\,dy \qquad (3)$$

where $r(x,y,t)$ is the reticle transmittance function and $s(x,y,t)$ is the two-dimensional input scene, i.e., what the missile sees. Due to the dimensionality, a mathematical analysis of Eq (3) is extremely difficult (Ref 4:54-57) and quickly leads to elegant formulas which obscure the basic concepts. Therefore, in order to simplify the mathematics

12
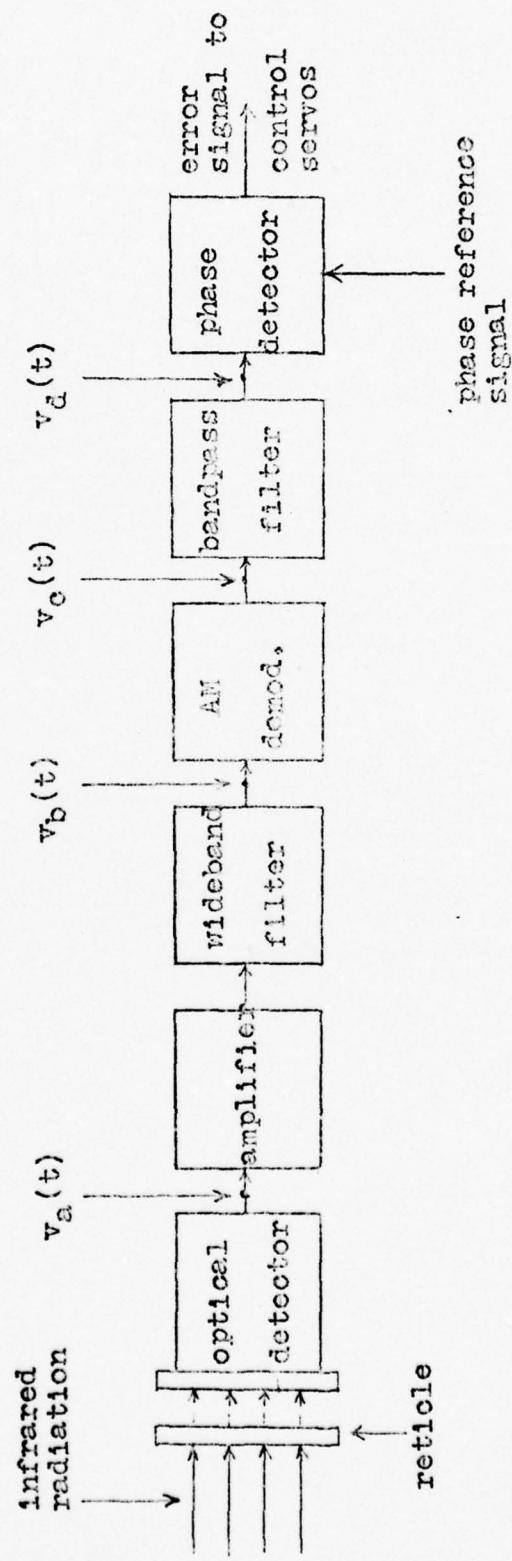
Figure 6. Block Diagram of Typical AM-Reticle System

13

without losing any basic concepts, a one-dimensional reticle analysis will be proposed using the following expression for the detector output

$$v_a(t) = \int_{-\infty}^{+\infty} r(x,t)s(x,t)dx \qquad (4)$$

where $r(x,t)$ is the one-dimensional reticle transmittance function and $s(x,t)$ is the one-dimensional scene function. Since the missile has a finite field of view, $s(x,t)$ will be bounded in x; thus, the limits of integration in Eq (4) would be across the field of view of the reticle system. However, in order to keep the analysis general, infinite limits are shown in Eq (4). The scene function, $s(x,t)$, is not assumed to be heavily time dependent; the time dependency has been shown to simplify later expressions when a time varying jammer is inserted into the analysis. Eq (4) shows one of the most important functions of a reticle, that of turning an essentially time-invariant scene function into a time varying electrical signal.

Figure 7 serves to illustrate the concept of a reticle transmittance function. As shown in Figure 7a, assume a small point source of infrared radiation is imaged on the reticle at point x_p; as the reticle rotates, the image is alternately passed and blocked by the transparent and opaque segments and one-half of the images' radiance is passed as the 0.5 transmittance section passes x_p. Figure 7b shows the fraction of total radiant flux passed by the reticle as

14
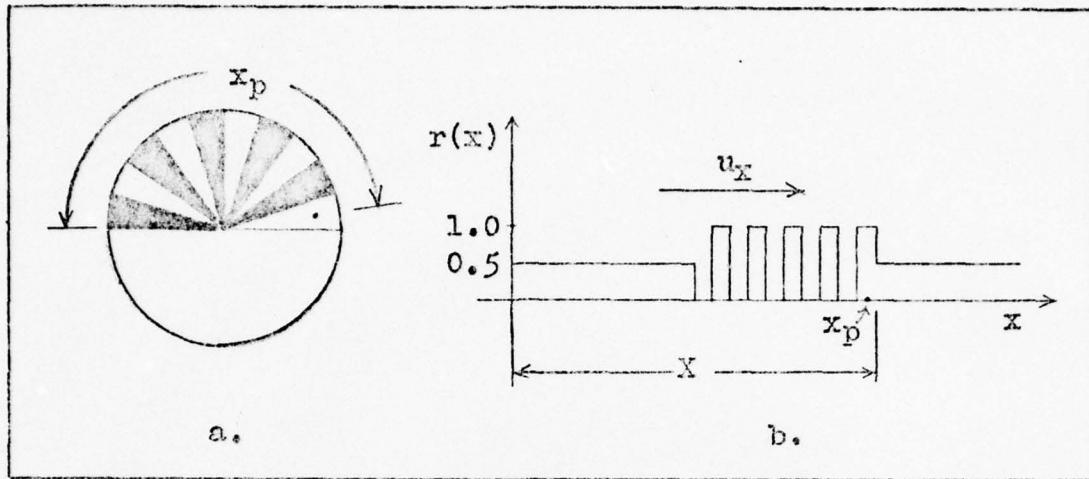
Figure 7. Reticle Transmittance Function

a function of position, this is the reticle transmittance function. To account for the circular rotation of the reticle in Figure 7a, the reticle transmittance function in Figure 7b is assumed to be infinite in extent with a period of X and linear velocity u_x in the x direction.

This one-dimensional model will account for the angular position of a target image on the reticle surface. It will not provide the radial position of the image. Figure 8 shows these positions. Recall from Chapter II, that the angular position of the target image is provided by the phase-modulated section of the reticle. Therefore, this one-dimensional model will attempt to relate the phase-modulation in $v_a(t)$ to the target position x_p.

To continue with the mathematical development, Eq (4) can be written as

$$v_a(t) = \int_{-\infty}^{+\infty} r(x - u_x t)s(x,t)dx \qquad (5)$$

15
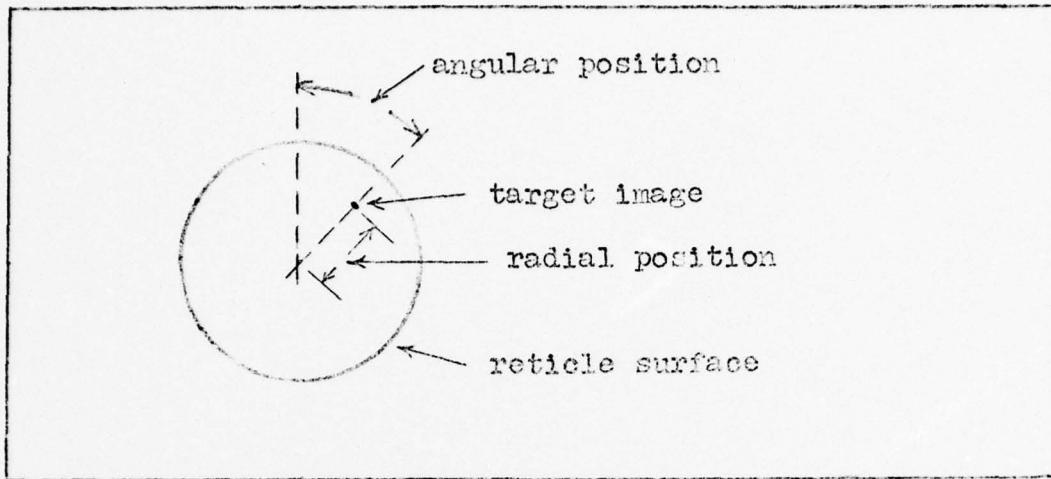
Figure 8. Reticle Diagram Showing Angular and Radial Position

where $r(x - u_x t)$ is the infinite reticle transmittance function moving with a velocity u_x in the x direction. Since the reticle transmittance function $r(x - u_x t)$ is periodic, it can be expanded into a Fourier series (Ref 6:43)

$$r(x - u_x t) = \sum_{n=-\infty}^{+\infty} c_n e^{j2\pi n f_0 (x-u_x t)} \qquad (6)$$

where the c_n's are the complex Fourier coefficients and $f_0 = 1/X$ where X is the reticle period.

Substituting Eq (6) into Eq (5) yields

$$v_a(t) = \int_{-\infty}^{+\infty} \left(\sum_{n=-\infty}^{+\infty} c_n e^{j2\pi n f_0 (x-u_x t)} \right) s(x,t) dx \qquad (7)$$

Assuming that the order of integration and summation can be exchanged, Eq (7) becomes

16

$$v_a(t) = \sum_{n=-\infty}^{+\infty} \left(c_n \, e^{-j2\pi nf_o u_x t} \int_{-\infty}^{+\infty} s(x,t) e^{j2\pi nf_o x} dx \right) \qquad (8)$$

The expression inside the integral in Eq (8) is the one-dimensional Fourier transform of $s(x,t)$ taken on x, or

$$\int_{-\infty}^{+\infty} s(x,t) e^{j2\pi nf_o x} dx = S(-nf_o, t) \qquad (9)$$

where $S(-nf_o, t)$ denotes the spatial Fourier transform of $s(x,t)$. Substituting Eq (9) into Eq (8) results in

$$v_a(t) = \sum_{n=-\infty}^{+\infty} c_n \, e^{-j2\pi nf_o u_x t} S(-nf_o, t) \qquad (10)$$

Now the frequency content of $v_a(t)$ will be found by taking the Fourier transform of both sides of Eq (10)

$$F\left[v_a(t)\right] = V_a(f) = \sum_{n=-\infty}^{+\infty} c_n F\left[e^{-j2\pi nf_o u_x t} S(-nf_o, t)\right] \qquad (11)$$

where $F[\cdot]$ indicates the Fourier transform of the argument. Recall that the multiplication of two functions in the time domain becomes a convolution in the frequency domain; therefore, Eq (11) becomes

$$V_a(f) = \sum_{n=-\infty}^{+\infty} c_n \left(F\left[e^{-j2\pi nf_o u_x t}\right] * F\left[S(-nf_o, t)\right] \right) \qquad (12)$$

17

where * denotes convolution. After substituting the following equations

$$F_t\left[e^{-j2\pi nf_o u_x t}\right] = \delta(f + nf_o u_x) \tag{13}$$

$$F_t\left[S(-nf_o, t)\right] = S(-nf_o, f) \tag{14}$$

into Eq (12), $V_a(\ )$ becomes

$$V_a(f) = \sum_{n=-\infty}^{+\infty} c_n\left[\delta(f + nf_o u_x) * S(-nf_o, f)\right] \tag{15}$$

where $\delta(\cdot)$ is the dirac delta or impulse function. In Eq (15) the reader should keep in mind that f denotes a "time" frequency (units of 1/sec), whereas f_o denotes a "spatial" frequency (units of 1/meters). After applying the sifting property of the impulse function, Eq (15) becomes

$$V_a(f) = \sum_{n=-\infty}^{+\infty} c_n\ S(-nf_o, f + nf_o u_x) \tag{16}$$

Eq (16) demonstrates that the frequency spectrum of the detector output is a discretely sampled version of the frequency spectrum of the scene function. For purposes of this analysis, a typical scene is composed of a target, a jammer, and a radiant background; thus an expression for s(x,t) may be written as follows

$$s(x,t) = A\ \delta(x - x_p) + b(x) + j(t)\delta(x - x_p) \tag{17}$$

18

where A $\delta(x - x_p)$ is a point source target located at point x_p with radiant power A, $b(x)$ is the space variant background scene, and $j(t)\delta(x - x_p)$ is a time-varying jammer collocated with the target. The two-dimensional (time and space) Fourier transform (Ref 6:50) of $s(x,t)$ is given by

$$S(f_x,f) = \int_{-\infty}^{+\infty} \int s(x,t)e^{-j2\pi(f_x x + ft)} \, dx \, dt \qquad (18)$$

where $S(f_x,f)$ is the two-dimensional Fourier transform with f_x denoting a spatial frequency and f denoting a temporal frequency. Substituting Eq (17) into Eq (18) and expanding yields

$$S(f_x,f) = \int_{-\infty}^{+\infty} \int A \, \delta(x-x_p)e^{-j2\pi(f_x x + ft)} \, dx \, dt$$

$$+ \int_{-\infty}^{+\infty} \int b(x)e^{-j2\pi(f_x x + ft)} \, dx \, dt$$

$$+ \int_{-\infty}^{+\infty} \int j(t)\delta(x - x_p)e^{-j2\pi(f_x x + ft)} \, dx \, dt \qquad (19)$$

After collecting common terms Eq (19) becomes

$$S(f_x,f) = A \int_{-\infty}^{+\infty} \delta(x - x_p)e^{-j2\pi f_x x} \, dx \int_{-\infty}^{+\infty} e^{-j2\pi ft} \, dt$$

$$+ \int_{-\infty}^{+\infty} b(x)e^{-j2\pi f_x x} \, dx \int_{-\infty}^{+\infty} e^{-j2\pi ft} \, dt$$

$$+ \int_{-\infty}^{+\infty} \delta(x - x_p)e^{-j2\pi f_x x} \, dx \int_{-\infty}^{+\infty} j(t)e^{-j2\pi ft} \, dt \qquad (20)$$

19

The terms under the integrals in Eq (20) are readily identifiable Fourier transforms; therefore, $S(f_x, f)$ becomes

$$S(f_x, f) = A\, e^{-j2\pi f_x x_p} \delta(f) + B(f_x)\delta(f) + J(f) e^{-j2\pi f_x x_p} \quad (21)$$

where $B(f_x)$ is the spatial Fourier transform of $b(x)$ and $J(f)$ is the temporal Fourier transform of $j(t)$.

Substituting Eq (21) into Eq (16) yields

$$V_a(f) = \sum_{n=-\infty}^{+\infty} c_n \left[A\, e^{+j2\pi nf_o x_p} \delta(f + nf_o u_x) \right.$$

$$+ B(-nf_o)\delta(f + nf_o u_x)$$

$$\left. + J(f + nf_o u_x) e^{+j2\pi nf_o x_p} \right] \quad (22)$$

Eq (22) represents the two-sided frequency spectrum of $v_a(t)$; the one-sided frequency spectrum of $v_a(t)$ can be found as follows

$$V_a(f) = \sum_{n=0}^{+\infty} \left(c_n \left[A\, e^{+j2\pi nf_o x_p} \delta(f + nf_o u_x) + B(-nf_o)\delta(f+nf_o u_x) \right.\right.$$

$$\left. + J(f+nf_o u_x) e^{+j2\pi nf_o x_p} \right] + c_{-n}\left[A\, e^{-j2\pi nf_o x_p} \delta(f - nf_o u_x) \right.$$

$$\left.\left. + B(nf_o)\delta(f-nf_o u_x) + J(f-nf_o u_x) e^{-j2\pi nf_o x_p} \right] \right) \epsilon_n$$

$$. \quad (23)$$

where $\epsilon_n = \begin{cases} 1, & n > 0 \\ \frac{1}{2}, & n = 0 \end{cases}$. The ϵ_n term is needed so that the

$n = 0$ term is not counted twice. After realizing that

$c_{-n} = c_n^*$ and after taking the inverse Fourier transform of

Eq (23), an expression for $v_a(t)$ can be written as follows

$$v_a(t) = F^{-1}[V_a(f)] = \sum_{n=0}^{+\infty} \left(c_n \left[A\, e^{+j2\pi n f_o x_p}\, e^{-j2\pi n f_o u_x t} \right. \right.$$

$$\left. + B(-nf_o) e^{-j2\pi n f_o u_x t} + j(t) e^{-j2\pi n f_o u_x t}\, e^{+j2\pi n f_o x_p} \right]$$

$$+ c_n^* \left[A\, e^{-j2\pi n f_o x_p}\, e^{j2\pi n f_o u_x t} + B(nf_o) e^{j2\pi n f_o u_x t} \right.$$

$$\left. \left. + j(t) e^{j2\pi n f_o u_x t}\, e^{-j2\pi n f_o x_p} \right] \right) \epsilon_n \tag{24}$$

In general, the Fourier coefficients, c_n, and the

Fourier transform of the background, $B(nf_o)$, are complex

quantities; as such they may be written in magnitude-phase

notation as follows

$$c_n = |c_n| e^{j\Theta_n} \tag{25}$$

$$B(nf_o) = |B(nf_o)| e^{j\phi_n} \tag{26}$$

$$B(-nf_o) = B^*(nf_o) = |B(nf_o)| e^{-j\phi_n} \tag{27}$$

21

Upon substituting Eqs (25), (26), and (27) into Eq (24), $v_a(t)$ becomes

$$v_a(t) = \sum_{n=0}^{+\infty} \left(|c_n| \left[A\ e^{-j(2\pi nf_o u_x t - 2\pi nf_o x_p - \theta_n)} \right. \right.$$

$$+ |B(nf_o)| e^{-j(2\pi nf_o u_x t + \phi_n - \theta_n)}$$

$$+ j(t)e^{-j(2\pi nf_o u_x t - 2\pi nf_o x_p - \theta_n)}$$

$$+ A\ e^{+j(2\pi nf_o u_x t - 2\pi nf_o x_p - \theta_n)}$$

$$+ |B(nf_o)| e^{+j(2\pi nf_o u_x t + \phi_n - \theta_n)}$$

$$\left. \left. + j(t)e^{+j(2\pi nf_o u_x t - 2\pi nf_o x_p - \theta_n)} \right] \right) \epsilon_n \qquad (28)$$

Recall that Euler's formula is given by

$$\cos \omega t = \frac{e^{j\omega t} + e^{-j\omega t}}{2} \qquad (29)$$

After substituting Eq (29) into Eq (28), $v_a(t)$ becomes

$$v_a(t) = \sum_{n=0}^{+\infty} \left(2\ A\ |c_n| \cos(2\pi nf_o u_x t - 2\pi nf_o x_p - \theta_n) \right.$$

$$+ 2|c_n||B(nf_o)| \cos(2\pi nf_o u_x t + \phi_n - \theta_n)$$

$$\left. + 2|c_n| j(t)\cos(2\pi nf_o u_x t - 2\pi nf_o x_p - \theta_n) \right) \epsilon_n \qquad (30)$$

Eq (30) represents the electrical output of the optical detector and as such is worth closer examination at this

point. Clearly, $v_a(t)$ is composed of a sum of sinusoidal components whose phase is determined by target position $(2\pi n f_o x_p)$, background radiance (ϕ_n), and reticle design (θ_n). The frequency of the components are harmonics of the scan rate of the reticle $(f_o u_x)$. Neglecting for the moment the jammer term, the amplitude of the sinusoidal components is, quite logically, affected by target intensity (A), background intensity $(|B(n f_o)|)$, and reticle design $(|c_n|)$. It would seem, at this early point at least, that this model has included the effects of the three major factors in the tracking problem, i.e., target, background, and the reticle. Now that an expression for the detector output has been found, the signal processing network of Figure 6 will be analyzed.

Analysis of Signal Processing Network

The amplifier in Figure 6 is used to amplify the small voltage output of the detector. Since this voltage gain will affect all components of $v_a(t)$ equally, the gain of the amplifier will be assumed to be unity. Indeed, the constant 2 found in front of each term in Eq (30) is superfluous and will be omitted in future discussions.

Jammer Model. Before the output of the wideband filter, $v_b(t)$, can be found, some assumption about $j(t)$ must be made. In the context of this report, the objective of jamming is to interfere with and cause erroneous operation of the missile's tracking system. In order to accomplish

23

this, the jamming waveform, $j(t)$, must influence $v_a(t)$ in such a manner as to cause erroneous phase information to be generated. Since $v_a(t)$ is composed of sinusoidal components, a logical first choice for $j(t)$ is to assume it sinusoidal also. Therefore, the assumption will be made that $j(t)$ is a sinusoid of frequency equal to the scan rate of the reticle; thus,

$$j(t) = H_j \cos(2\pi f_o u_x t + \theta_j) + H_{DC} \qquad (31)$$

where H_j is the jammer power found in the frequency component at the reticle scan frequency, θ_j is the phase angle of the jammer relative to the reticle, and H_{DC} is the DC or constant component of the jammer. The H_{DC} term is needed because $j(t)$ is a time-varying radiant power waveform which must be always positive. For a simple, single-frequency jammer operating at the scan rate of the reticle, H_j and H_{DC} would be equal, thus producing an instantaneous peak jammer power of $2H_j$. Later in this paper, several multiple frequency waveforms will be analyzed by computing H_j and H_{DC} for each waveform.

Now that an expression for $j(t)$ has been found, $v_a(t)$ can be written as

$$v_a(t) = \sum_{n=0}^{+\infty} (|c_n| [A \cos(2\pi n f_o u_x t - 2\pi n f_o x_p - \theta_n)$$

$$+ | B(n f_o) | \cos(2\pi n f_o u_x t + \phi_n - \theta_n)$$

$$+ (H_j \cos(2\pi f_o u_x t + \theta_j) + H_{DC}) \cos(2\pi n f_o u_x t - 2\pi n f_o x_p - \theta_n)]) \epsilon_n$$

$$(32)$$

24

Eq (32) can be simplified by use of a trigonometric identity to yield

$$v_a(t) = \sum_{n=0}^{+\infty} \left\{ |c_n| [(A + H_{DC}) \cos(2\pi n f_o u_x t - 2\pi n f_o x_p - \theta_n) \right.$$

$$+ |B(n f_o)| \cos(2\pi n f_o u_x t + \phi_n - \theta_n)$$

$$+ \frac{H_j}{2} \cos(2\pi(n+1) f_o u_x t - 2\pi n f_o x_p + \theta_j - \theta_n)$$

$$\left. + \frac{H_j}{2} \cos(2\pi(n-1) f_o u_x t - 2\pi n f_o x_p - \theta_j - \theta_n)] \right\} c_n \qquad (33)$$

Eq (33) can now be taken through the wideband filter shown in Figure 6.

Effects of Wideband Filter. The wideband filter serves two purposes. First, its' passband is such that it passes the carrier frequency produced by the fan-shaped segments of the reticle (see Figure 4) and the frequency harmonic directly above this one. This upper frequency is analogous to an upper sideband frequency in communication terminology (Ref 7:93-112; Ref 8:203-228). (Note: A double sideband analysis may be carried out by making the filter wider. The results are the same.) The reader should keep in mind that the desired positional information is carried by the sideband frequency, i.e., envelope of the carrier, and not by the carrier itself, this fact will become obvious later.

The second purpose, actually a consequence of the first, is to filter out the effects of the background radiation. As stated in Chapter II, if the carrier frequency is

typically greater than eight times the fundamental scan frequency, then essentially no component of $v_a(t)$ is due to background radiation. Therefore, the assumption will be made that the carrier frequency is at least eight times the scan rate of the reticle.

The wideband filter output, $v_b(t)$, will consist of six components, three at the carrier frequency and three at the sideband frequency. An expression for $v_b(t)$ is shown below

$$v_b(t) = (A+H_{DC})|c_{n_f}|\cos(2\pi n_f f_o u_x t - 2\pi n_f f_o x_p - \theta_{n_f})$$

$$+ (A+H_{DC})|c_{n_f+1}|\cos[2\pi(n_f+1)f_o u_x t - 2\pi(n_f+1)f_o x_p - \theta_{n_f+1}]$$

$$+ \frac{H_j}{2}|c_{n_f-1}|\cos[2\pi n_f f_o u_x t - 2\pi(n_f-1)f_o x_p - \theta_{n_f-1} + \theta_j]$$

$$+ \frac{H_j}{2}|c_{n_f+1}|\cos[2\pi n_f f_o u_x t - 2\pi(n_f+1)f_o x_p - \theta_{n_f+1} - \theta_j]$$

$$+ \frac{H_j}{2}|c_{n_f}|\cos[2\pi(n_f+1)f_o u_x t - 2\pi n_f f_o x_p - \theta_{n_f} + \theta_j]$$

$$+ \frac{H_j}{2}|c_{n_f+2}|\cos[2\pi(n_f+1)f_o u_x t - 2\pi(n_f+2)f_o x_p - \theta_{n_f+2} - \theta_j]$$

$$(34)$$

where n_f is the carrier harmonic. Eq (34) can be simplified by letting

$$2\pi n_f f_o u_x = \omega_c \tag{35}$$

$$2\pi f_o u_x = \omega_m \tag{36}$$

26

Substitution of Eq (35) and Eq (36) into Eq (34) results in

$$v_b(t) = (A+H_{DC})|c_{n_f}|\cos(\omega_c t - 2\pi n_f f_o x_p - \theta_{n_f})$$

$$+ \frac{H_j}{2}|c_{n_f-1}|\cos[\omega_c t - 2\pi(n_f-1)f_o x_p - \theta_{n_f-1} + \theta_j]$$

$$+ \frac{H_j}{2}|c_{n_f+1}|\cos[\omega_c t - 2\pi(n_f+1)f_o x_p - \theta_{n_f+1} - \theta_j]$$

$$+ (A+H_{DC})|c_{n_f+1}|\cos[(\omega_c+\omega_m)t - 2\pi(n_f+1)f_o x_p - \theta_{n_f+1}]$$

$$+ \frac{H_j}{2}|c_{n_f}|\cos[(\omega_c+\omega_m)t - 2\pi n_f f_o x_p - \theta_{n_f} + \theta_j]$$

$$+ \frac{H_j}{2}|c_{n_f+2}|\cos[(\omega_c+\omega_m)t - 2\pi(n_f+2)f_o x_p - \theta_{n_f+2} - \theta_j]$$

$$(37)$$

Demodulation. The demodulation process is accomplished by multiplying $v_b(t)$ by a sinusoid of frequency ω_c and in phase with the carrier. The following expression can be written for the output of the demodulator

$$v_c(t) = v_b(t)[\cos(\omega_c t - 2\pi n_f f_o x_p - \theta_{n_f})] \qquad (38)$$

Since the jammer is operating at the scan rate of the reticle, an assumption implicit in Eq (38) is that the jammer will have little effect upon the phase of the carrier. The tedium of actually multiplying Eq (38) out can be avoided by

27

recalling that multiplication by the cosine term serves to translate the frequency spectrum of $v_b(t)$ up and down the frequency axis by an amount equal to ω_c (Ref 8:224-225). Therefore, the following expression can be written

$$v_c(t) = (A+H_{DC})|c_{n_f}| + \frac{H_j}{2}|c_{n-1 \atop f}|\cos(2\pi f_o x_p + \theta_j - \theta_1)$$

$$+ \frac{H_j}{2}|c_{n+1 \atop f}|\cos(-2\pi f_o x_p - \theta_j - \theta_2)$$

$$+ (A+H_{DC})|c_{n+1 \atop f}|\cos(\omega_m t - 2\pi f_o x_p - \theta_2)$$

$$+ \frac{H_j}{2}|c_{n_f}|\cos(\omega_m t + \theta_j)$$

$$+ \frac{H_j}{2}|c_{n+2 \atop f}|\cos(\omega_m t - 4\pi f_o x_p - \theta_j - \theta_3)$$

$$+ (2^{nd} \text{ harmonic of carrier and sideband}) \qquad (39)$$

where $\theta_1 = \theta_{n-1 \atop f} - \theta_{n_f}$, $\theta_2 = \theta_{n+1 \atop f} - \theta_{n_f}$, and $\theta_3 = \theta_{n+2 \atop f} - \theta_{n_f}$.

Bandpass Filter. The bandpass filter shown in Figure 6 is designed to pass only those components of $v_c(t)$ at frequency ω_m. That is, the DC and 2nd harmonic terms of $v_c(t)$ are rejected by the bandpass filter resulting in

$$v_d(t) = (A+H_{DC})|c_{n+1 \atop f}|\cos(\omega_m t - 2\pi f_o x_p - \theta_2)$$

$$+ \frac{H_j}{2}|c_{n_f}|\cos(\omega_m t + \theta_j)$$

$$+ \frac{H_j}{2}|c_{n+2 \atop f}|\cos(\omega_m t - 4\pi f_o x_p - \theta_j - \theta_3) \qquad (40)$$

28

Additional simplifying assumptions can be made about $v_d(t)$ by examining the Fourier coefficients c_{n+1_f}, c_{n_f}, and c_{n+2_f} found in Eq (40). As explained in Chapter II, one of the most important functions of a reticle is that it acts as a spatial filter. A spatial filter may be likened to an electronic filter with the spatial filter passing or rejecting spatial frequencies rather than temporal frequencies. Similarly, a spatial filter may be thought of as having a spatial passband composed of those spatial frequencies passed by a particular reticle. For example, the AM-reticle illustrated in Figure 7a can be shown to have a spatial passband consisting of the carrier spatial frequency (i.e., c_{n_f}) and the sideband frequencies on either side of the carrier (i.e., c_{n-1_f} and c_{n+1_f}). (Note: The reticle also passes the DC component, C_o). In other words, the amplitude of all spatial frequencies except c_{n_f}, c_{n-1_f}, and c_{n+1_f} is negligible. (This tedious but straightforward analysis is omitted here.) Thus, for purposes of this thesis, it is assumed that a properly designed AM-reticle will have a passband consisting of the carrier spatial frequency and the sideband frequencies on either side of the carrier.

With the above assumption having been made, $|c_{n+2_f}|$ in Eq (40) is assumed to be very small in relation to either $|c_{n_f}|$ or $|c_{n+1_f}|$; therefore, $v_d(t)$ can be written as

$$v_d(t) = (A+H_{DC})|c_{n+1_f}|\cos(\omega_m t - 2\pi f_o x_p - \Theta_2)$$

$$+ \frac{H_j}{2}|c_{n_f}|\cos(\omega_m t + \Theta_j) \tag{41}$$

System Operation Without Jamming

Assume for the moment that no jammer is present; therefore, Eq (41) becomes

$$v_d(t) = A|c_{n+1_f}|\cos(\omega_m t - 2\pi f_o x_p - \Theta_2) \tag{42}$$

Under normal operation (without jamming), the electrical signal represented by Eq (42) is fed into a phase discriminator (see Figure 6) where it is compared against a reference signal to determine the relative phase of $v_d(t)$. This relative phase angle, given by the term $2\pi f_o x_p$, contains information regarding the position of the target, x_p. An error signal proportional to the relative phase of $v_d(t)$ and hence to the target position is generated and subsequently used to position the missile's control fins.

System Operation With Jamming

Notice what effect the addition of the jammer has on system operation; Eq (41) is repeated here for convenience

$$v_d(t) = (A+H_{DC})|c_{n+1_f}|\cos(\omega_m t - 2\pi f_o x_p - \Theta_2)$$

$$+ \frac{H_j}{2}|c_{n_f}|\cos(\omega_m t + \Theta_j) \tag{41}$$

The term containing the target position, x_p, is still
present, in fact it has been reinforced by the DC power of
the jammer. However, a new term due solely to the jammer
has been added; this jammer term has a phase angle deter-
mined exclusively by the relative phase between the reticle
and the jammer. The output of the phase discriminator will
now be proportional to the composite phase of the two terms
in Eq (41). If this composite phase is significantly
different from the actual target phase angle, then a miss or
at least a momentary "look-away" by the IR missile can be
expected.

IV. Smart Jamming

For purposes of this thesis, smart jamming is defined
as an attempt to degrade the tracking performance of an IR
system by exploiting a general knowledge about that system.
The system characteristic exploited in this chapter is the
phase information used by an AM-reticle system for tracking.

This chapter will investigate two forms of smart jamming:
sinusoidal jamming and noise jamming. Also, a methodology for
evaluating the effects of each form will be presented.

Sinusoidal Jamming

The mathematical model developed in Chapter III demon-
strated that a reticle-based IR system can be jammed (i.e.,
its tracking performance degraded) by an IR source sinu-
soidally-modulated at a frequency equal to the scan rate of
the reticle. Thus, a tacit assumption was made that the
scan rate of the reticle is known. This assumption is
unrealistic for two reasons. First, a potential enemy may
possess several IR missiles, both ground-launched and air-
launched, that operate at different scan rates. Secondly,
due to gyro spin driftdown, the spin frequency of a reticle
decays slowly after the missile is launched. Thus, to insure
maximum flexibility against various missile types, an effec-
tive jamming system must be capable of jamming over a fre-
quency band.

Sinusoidal jamming over a desired frequency band can be
accomplished by periodic jamming codes which have line fre-
quency spectrums covering the desired band. Figure 9 illus-
trates this concept, where $J(f)$ is the frequency spectrum of
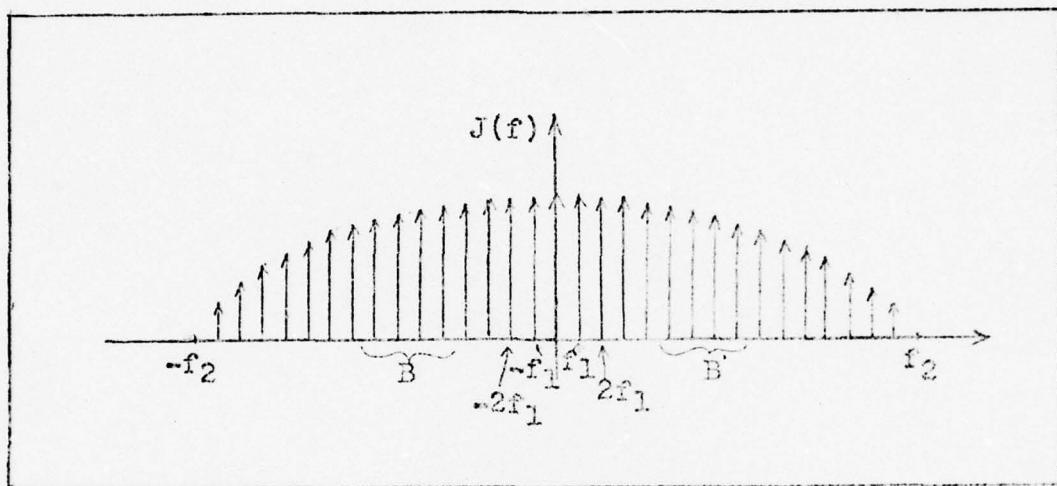
Figure 9. Sinusoidal Jamming over a Frequency Band

the jamming waveform $j(t)$. With reference to Figure 9, sev-
eral definitions concerning sinusoidal jamming will be made.
The frequency spread or bandwidth of the jamming signal is
defined as the frequency where the amplitude of the indi-
vidual frequency components become nearly zero. For the
example shown in Figure 9, the bandwidth of the coded signal
is f_2. The frequency spacing is defined as the interval
between frequency components, e.g., the frequency spacing in
Figure 9 is f_1. In order to simplify later calculations, all
codes are assumed to be frequency spaced so that only one
frequency component is filtered by the network shown in
Figure 6. However, no knowledge is assumed about which

33

particular component is filtered. Another useful description
of the frequency content of a code is the number of sinu-
soidal components prior to f_2; this number is a crude measure
of how well a code "covers" a particular frequency band.

The frequency band denoted as B in Figure 9 is assumed
to contain all commonly encountered reticle scan rates. In
other words, the individual scan rates are assumed unknown,
but the frequency band in which they lie is assumed known.

Development of Phase Error Expression

With the discussion of sinusoidal jamming completed, an
error expression for the phase of a sinusoidally jammed
reticle system will now be derived. From Chapter III, the
expression used for tracking purposes is Eq (41)

$$v_d(t) = (A + H_{DC})|c_{n+1_f}|\cos(\omega_m t - 2\pi f_o x_p - \theta_2)$$
$$+ \frac{H_j}{2}|c_{n_f}| \cos(\omega_m t + \theta_j) \tag{41}$$

Eq (41) is shown graphically in Figure 10 as a phasor diagram.

As stated in Chapter III, the tracking system of the
missile will track the composite phase, θ_e, of the two terms
in Eq (41), rather than the correct phase, θ_p. Referring to
Figure 10, an expression for the magnitude of the composite
phase, θ_e, may be written as

$$\theta_e = \arctan \left[\frac{\frac{H_j}{2}|c_{n_f}|\sin\theta_j + (A+H_{DC})|c_{n+1_f}|\sin\theta_p}{\frac{H_j}{2}|c_{n_f}|\cos\theta_j + (A+H_{DC})|c_{n+1_f}|\cos\theta_p} \right] \tag{43}$$

34
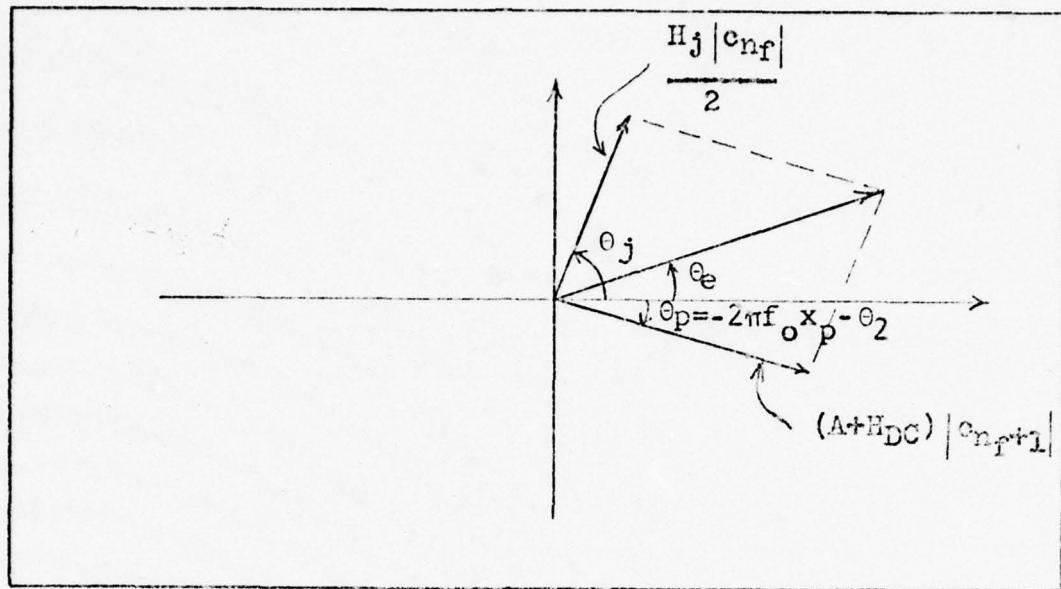
Figure 10. Phasor Diagram Showing Phase Error Due to Jamming

Since Θ_e will be used as a comparison parameter for jamming techniques and not to predict the actual system tracking error and since a reticle will affect all jamming codes in a similar fashion, it will be assumed that $|c_{n_f}| \approx |c_{n+1_f}|$. Therefore, Eq (43) becomes

$$\Theta_e = \text{arc tan} \left[\frac{\frac{H_j}{2} \sin \Theta_j + (A+H_{DC}) \sin \Theta_p}{\frac{H_j}{2} \cos \Theta_j + (A+H_{DC}) \cos \Theta_p} \right] \qquad (44)$$

Now, let

$$\Theta_j = \Theta_p + \Theta_r \qquad (45)$$

where Θ_r is the relative phase angle between Θ_j and Θ_p.

35

Substituting Eq (45) into Eq (44) yields

$$\theta_e = \arctan \left[\frac{\frac{H_j}{2} \sin(\theta_p + \theta_r) + (A + H_{DC}) \sin \theta_p}{\frac{H_j}{2} \cos(\theta_p + \theta_r) + (A + H_{DC}) \cos \theta_p} \right] \quad (46)$$

After the application of a basic trigonometric identity, Eq (46) becomes

$$\theta_e = \arctan \left[\frac{\frac{H_j}{2}(\sin\theta_p \cos\theta_r + \cos\theta_p \sin\theta_r) + (A + H_{DC})\sin\theta_p}{\frac{H_j}{2}(\cos\theta_p \cos\theta_r - \sin\theta_p \sin\theta_r) + (A + H_{DC})\cos\theta_p} \right]$$

$$(47)$$

From the standpoint of jamming effectiveness, only the relative phase, θ_r, between the jammer and the reticle is of concern. Therefore, it is assumed that $\theta_p = 0$; now θ_e becomes a measure of the phase error induced by jamming. This assumption results in

$$\theta_e = \arctan \left[\frac{H_j \sin \theta_r}{H_j \cos \theta_r + 2(A + H_{DC})} \right] \quad (48)$$

From Eq (48) it is clear that the phase error due to sinusoidal jamming, θ_e, is heavily dependent upon the relative phase of the jammer, θ_r. However, since θ_r is determined with reference to a signal generated internally to the IR missile, it is assumed that θ_r can not be measured by the jammer. Therefore, to remove the dependency of θ_e upon θ_r,

36

an optimal value of θ_r will be found which maximizes θ_e. For purposes of code comparison, it is assumed that all jamming codes are operating at this optimal value of θ_r.

This optimal value of θ_r is found as follows. The derivative with respect to θ_r of the argument of the arc tan function in Eq (48) will be taken. This operation yields

$$\frac{d}{d\theta_r}\left[\frac{H_j \sin\theta_r}{H_j \cos\theta_r + 2(A+H_{DC})}\right] =$$

$$\frac{H_j \cos\theta_r[H_j \cos\theta_r + 2(A+H_{DC})] + H_j^2 \sin^2\theta_r}{[H_j \cos\theta_r + 2(A+H_{DC})]^2} \qquad (49)$$

The right-hand side of Eq (49) will be set equal to zero in order to maximize θ_e with respect to θ_r; thus, Eq (49) becomes

$$H_j^2 \cos^2\theta_r + 2(A+H_{DC})H_j \cos\theta_r + H_j^2 \sin^2\theta_r = 0 \qquad (50)$$

Solving for θ_r results in

$$\theta_{r,\,max} = \cos^{-1}\left[\frac{-H_j}{2(A+H_{DC})}\right] \qquad (51)$$

where $\theta_{r,\,max}$ is the value of θ_r that maximizes θ_e.

Now, let

$$H_j = \alpha H \qquad (52)$$

$$H_{DC} = \beta H \qquad (53)$$

$$\frac{H}{A} = \frac{J}{S} \qquad (54)$$

37

where H is the peak jammer power, α is the fraction of the peak jammer power in the desired frequency component of the code, β is the fraction of the peak jammer power in the DC term of the code, and (J/S) is the ratio of the peak jammer power to the average power of the target. The term (J/S) is commonly referred to as the jammer-to-signal ratio or just simply the J-to-S ratio. Substituting Eqs (52), (53), and (54) into Eq (51) yields

$$\theta_{r,max} = \cos^{-1}\left[\frac{-\alpha\left(\frac{J}{S}\right)}{2\left(1 + \beta\left(\frac{J}{S}\right)\right)}\right] \tag{55}$$

Substituting Eqs (52), (53), and (54) into Eq (48) results in

$$\theta_e = \arctan\left[\frac{\alpha\left(\frac{J}{S}\right)\sin\theta_r}{\alpha\left(\frac{J}{S}\right)\cos\theta_r + 2\left(1 + \beta\left(\frac{J}{S}\right)\right)}\right] \tag{56}$$

In order to substitute Eq (55) into Eq (56) a value for $\sin\theta_r$ is needed; this value can be found by graphical means as shown in Figure 11. As can be seen from Figure 11, an expression for $\sin\theta_r$ can be written as

$$\sin\theta_r = \frac{\sqrt{\left[2\left(1+\beta\left(\frac{J}{S}\right)\right)\right]^2 - \left[\alpha\left(\frac{J}{S}\right)\right]^2}}{2\left[1 - \beta\left(\frac{J}{S}\right)\right]} \tag{57}$$

38
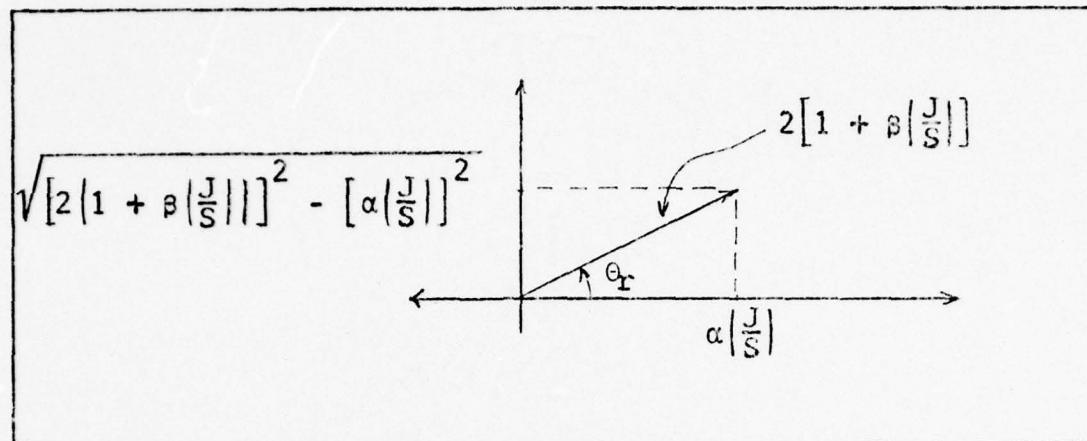
Figure 11. Graphical Determination of $\sin \Theta_r$

Substitution of Eq (55) and Eq (57) into Eq (56) yields

$$\Theta_e = \text{arc tan} \left[\frac{\dfrac{\alpha\left|\frac{J}{S}\right| \sqrt{\left[2\left|1+\beta\left|\frac{J}{S}\right|\right|\right]^2 - \left[\alpha\left|\frac{J}{S}\right|\right]^2}}{2\left[1+\beta\left|\frac{J}{S}\right|\right]}}{\alpha\left|\frac{J}{S}\right|\left[\dfrac{-\alpha\left|\frac{J}{S}\right|}{2\left|1+\beta\left|\frac{J}{S}\right|\right|}\right] + 2\left[1+\beta\left|\frac{J}{S}\right|\right]} \right] \quad (58)$$

Simplification of Eq (58) results in

$$\Theta_e = \text{arc tan} \frac{\alpha\left|\frac{J}{S}\right|}{\sqrt{\left[2\left|1+\beta\left|\frac{J}{S}\right|\right|\right]^2 - \left[\alpha\left|\frac{J}{S}\right|\right]^2}} \quad (59)$$

Eq (59) expresses Θ_e in terms of the code parameters α and β and the jammer parameter (J/S); thus, Eq (59) is the desired expression for Θ_e. For a given (J/S) ratio, Eq (59) will provide a convenient method of comparison between different jammer modulation schemes.

39

A plot of Eq (59) will show in visual terms the relationship between Θ_e and α, β, and (J/S). Such plots are shown in Figures 12 and 13. Figure 12 is drawn for an arbitrary value of $\beta = .05$ and Figure 13 is drawn for an arbitrary value of $\beta = .025$. In each graph it is apparent that Θ_e is a monotonically increasing function of both α and (J/S).

Also from Figures 12 and 13, it is clear that for a given α and (J/S), an increase in the DC component of the code, β, results in a decrease in Θ_e. This is to be expected since the DC value of the jammer aids the missile in tracking its target.

The curves shown in Figures 12 and 13 allow a basic conclusion to be made about an effective jamming code. This conclusion states that the sinusoidal component of the code at the harmonic being tracked by the missile should be as high as possible relative to the average or DC component of the code. The overall code, however, must still remain non-negative, as negative IR radiance is not possible. This fact is a significant problem in trying to reduce the DC component while increasing the AC components.

In regard to the effect of (J/S) on Θ_e, Figure 12 is redrawn with an expanded (J/S) axis in Figure 14. If the code parameters α and β are held constant, Figure 14 demonstrates that an increase in (J/S) results in an increase in Θ_e. The jammer-to-signal ratio is not a parameter of the particular modulation technique, rather it is determined by

α = .1

α = .08

α = .06

α = .04

α = .02

25

20

15

10

5

(J/G) ratio

40

30

20

10

0

Relative Phase Error (degrees)
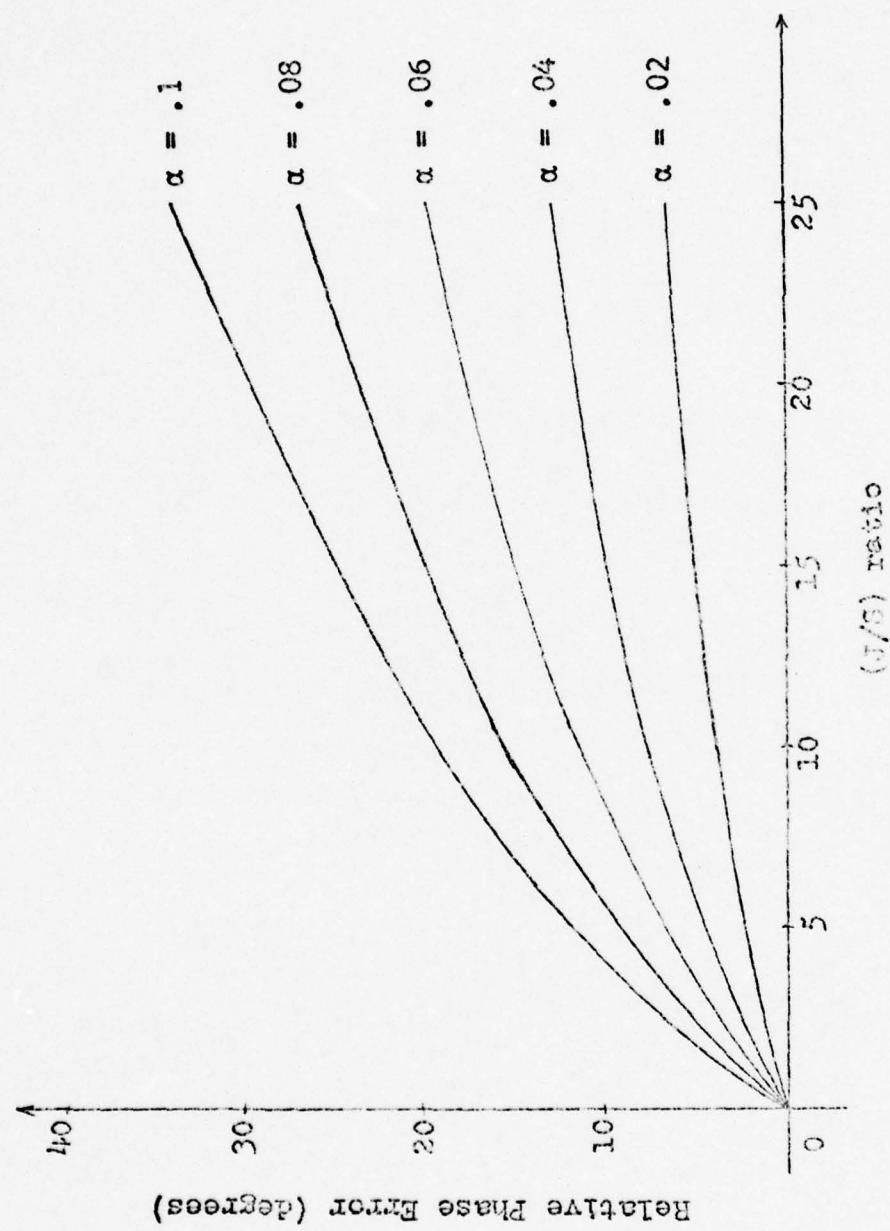
Figure 12. Phase Error Curve for β = .05

41

Figure 13. Phase Error Curve for $\beta = .025$

42

α = .1

(J/S) ratio

100   80   60   40   20

Relative Phase Error (degrees)

60   40   20   0
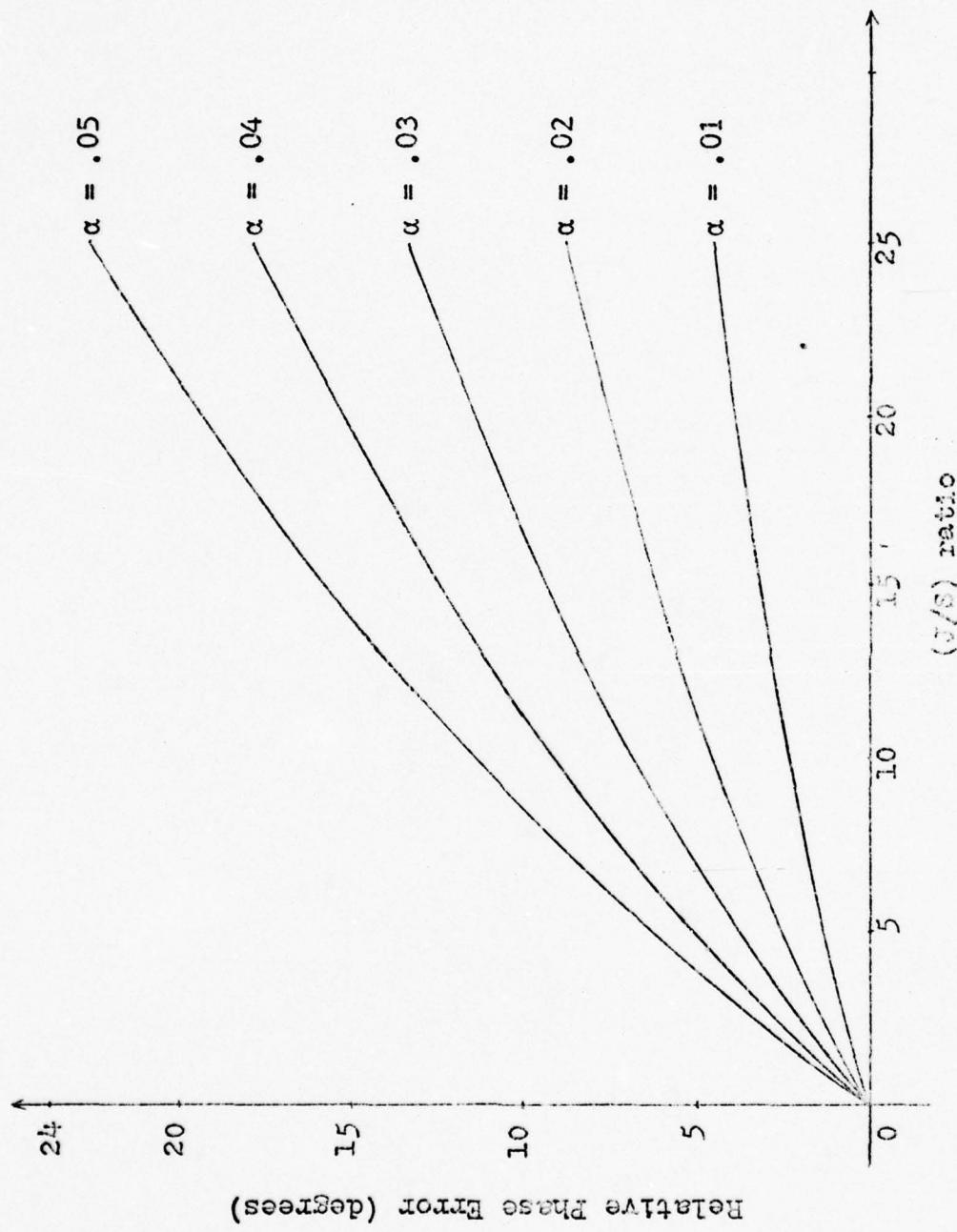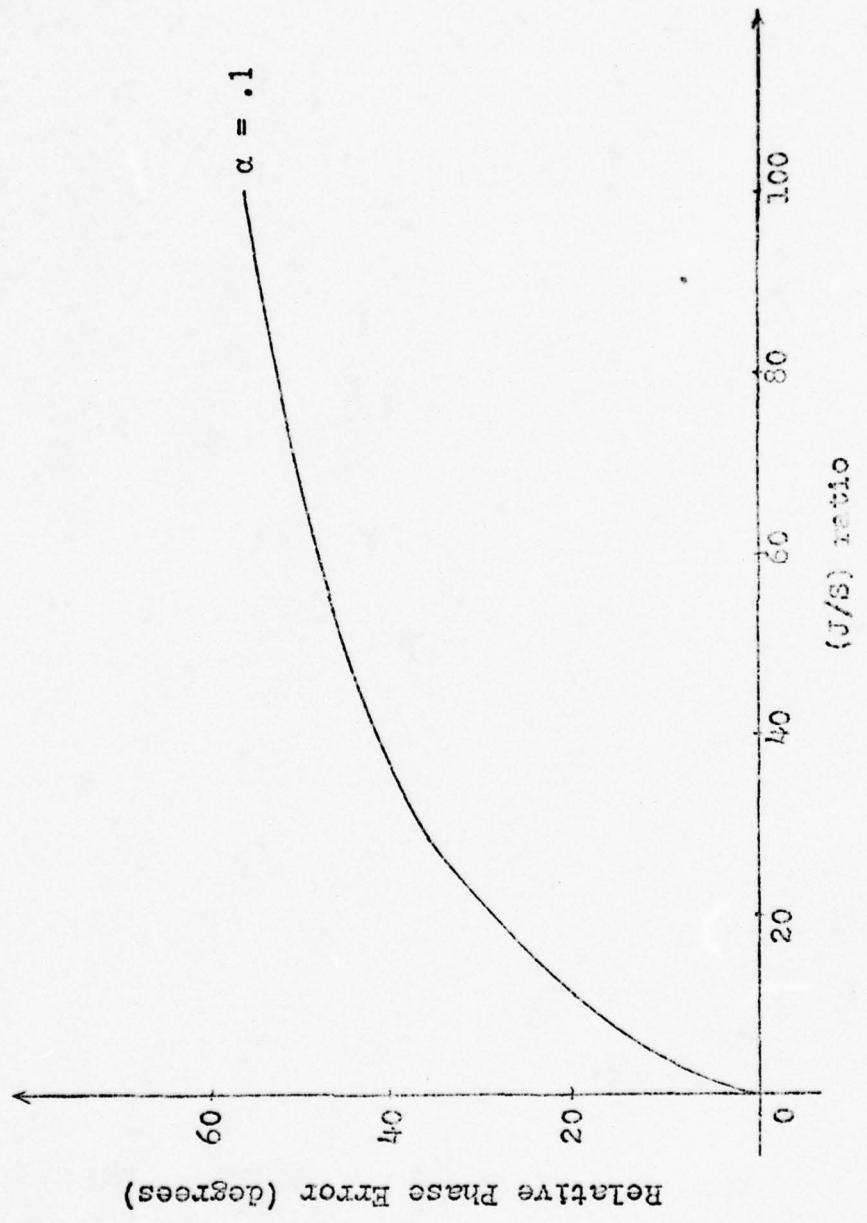
Figure 14. Expanded Phase-Error Curve (ε = .05)

43

the peak power of the IR device and the average power of the target. Therefore, as far as smart jamming is concerned, Figure 14 demonstrates the need for infrared sources with high peak power. The question of whether or not such IR sources exist now or will exist in the near future is not within the scope of this thesis.

Noise Jamming

As will be shown in Chapter V, some jamming codes have frequency spectrums which are continuous (i.e., not a line spectrum). Clearly, this type of spectrum does not fit the sinusoidal model presented in the previous section; therefore, in this section, a continuous spectrum code will be modeled as an additive noise source. The analysis in this section is intended as a crude, first-cut attempt at analyzing noise jamming; consequently, many liberties have been taken in the mathematical analysis.

Noise Model. A continuous spectrum code is assumed to act as an additive noise source in the IR system shown in Figure 6. In order to show the effects of a noise source on the phase tracking performance of an IR system, assume that the network of Figure 15 is inserted between the bandpass filter and the phase detector in Figure 6. This network is added for two reasons. First, in a practical sense the addition of a phase-lock loop (PLL) can result in better phase measurement, particularly at low signal-to-noise ratios (Ref 7:285-289). Secondly, the noise performance of

44
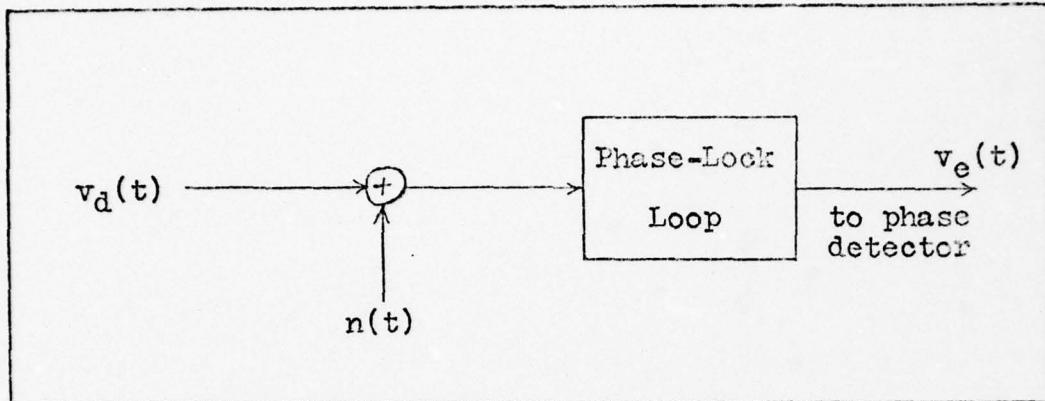
Figure 15. Network Showing Noise Source Due to Jamming

a PLL is readily available in the literature (Ref 7:127-132;
Ref 12:28-36).

In the absence of noise and with the PLL in lock, the
output phase of $v_e(t)$ is a good measure of the phase of
$v_d(t)$; however, when a noise source is added, the phase of
$v_e(t)$ can be considerably different from that of $v_d(t)$.
Thus, the noise jammer has caused a phase error in the out-
put of the PLL. The variance of this phase error can be
shown to be (Ref 12:35)

$$\sigma_{\theta_n}^2 = \frac{NB_L}{A_d^2} \tag{60}$$

where $\sigma_{\theta_n}^2$ is the variance of the phase error, N is the one-
sided amplitude of the power spectral density of the noise,
B_L is the loop bandwidth of the PLL, and A_d is the amplitude
of $v_d(t)$.

45

In a crude sense, the square root of the phase error variance is a measure of the rms magnitude of the phase error itself, or

$$\Theta_n \approx \left[\sigma^2_{\Theta_n}\right]^{\frac{1}{2}} = \left[\frac{NB_L}{A_d^2}\right]^{\frac{1}{2}} \tag{61}$$

where Θ_n is the rms magnitude of the phase error. A plot of Eq (61) is found in Figure 16. More will now be said about relating N and B_L to system parameters.

Assume that the power spectral density of $n(t)$ is as shown in Figure 17. From Eq (41), it is clear that the PLL is tracking a frequency of ω_m which is the scan frequency of the reticle. Since the jamming code is assumed to have a
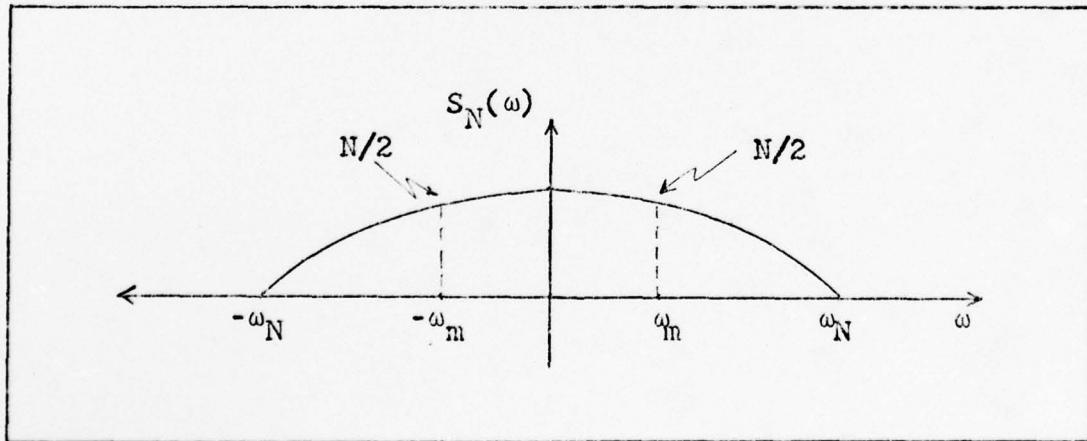
Figure 17. Sample Power Spectral Density of n(t)

bandwidth of $\omega_h > \omega_m$, then ω_m will lie as shown in Figure 17. If the loop bandwidth, B_L, is small relative to ω_n, then the

46
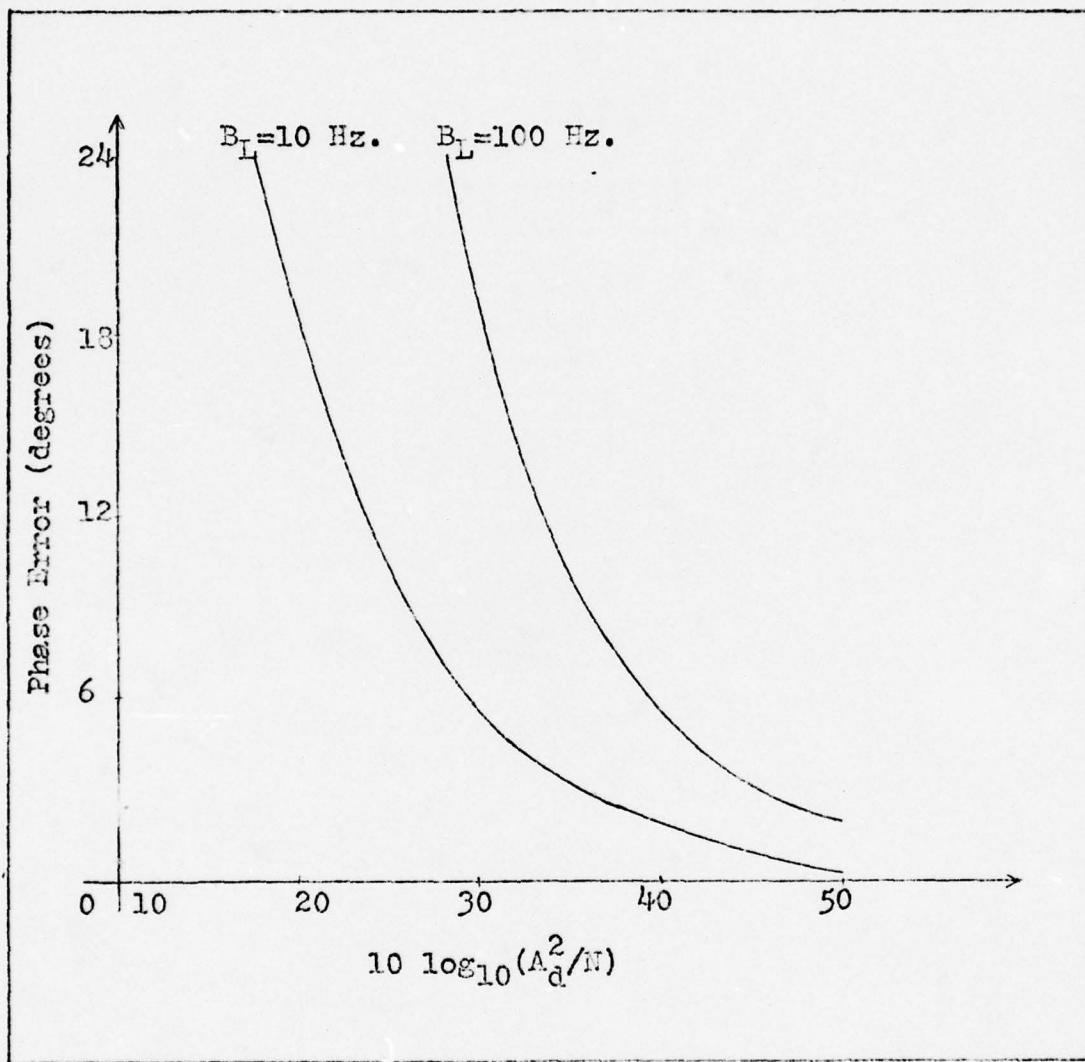
Figure 16. Phase Error Due to Noise Jamming vs. Signal-to-Noise Ratio

value of $S_n(\omega)$ evaluated at ω_m is $N/2$. This is the two-sided amplitude of the noise power; the one-sided amplitude is found by multiplying by 2.

The loop bandwidth is a parameter of the PLL and can be determined as follows. The phase of $v_d(t)$ is in actuality a time varying quantity; therefore, $v_d(t)$ will have some finite bandwidth determined by how fast its' phase changes. Thus, in order to track $v_d(t)$ without distortion, the PLL must have a bandwidth wide enough to pass $v_d(t)$; this bandwidth is B_L.

Total System Phase Error. For codes which have both continuous and line spectra, the magnitude of the total phase error will be obtained by simply adding the magnitude of the phase error due to the noise jamming to the magnitude of the phase error due to the sinusoidal jamming. Thus, the total phase error is given by

$$\Theta_T = \Theta_e + \Theta_N \tag{62}$$

where Θ_T is the magnitude of the total phase error.

48

V.   Coded Modulation Techniques

In this chapter several coded modulation techniques for use by IR jammers against reticle-based IR systems will be proposed. They include periodic, pseudorandom, and random binary modulation. The phase error expressions developed in Chapter IV will serve as a basis for comparing modulation techniques. This chapter will begin by summarizing the desirable code properties discussed in previous chapters.

Summary of Code Requirements

Since only the intensity of the IR radiation is modulated, the first and most severe constraint on any perspective modulation technique is that it must be non-negative. Because of this limitation, any feasible code will have a non-zero average or DC value.

Secondly, since the DC value of the code helps the IR missile to track the target, as much as possible of the code's total power must be in its sinusoidal or AC components. It is these sinusoidal components that can cause erroneous tracking information to be generated by the tracking system. Thirdly, because the reticle scan rate is assumed to be unknown, an effective code must spread its energy over a frequency band which covers all or most reticle scan rates. The actual scan rates are classified, and hence will not be discussed in this report.

49

Method of Investigation

For codes containing only a line spectrum, the first step in the evaluation process will consist of finding an expression for the frequency spectrum. Once the frequency spectrum has been determined then the amplitude of the desired harmonic can be found; this amplitude expressed as a fraction of the code's peak power is the α factor discussed in Chapter IV. The DC value of the code expressed as a fraction of the peak power is the β factor also discussed in Chapter IV. After α and β have been found, then Eq (59) will be used to find the relative phase angle error for each frequency component of the code. For codes having continuous frequency spectrums, Eq (61) will be used to determine the phase error due to noise jamming.

The jamming codes will be compared using only one (J/S) ratio. This is because the J-to-S ratio is a system parameter and not a code parameter. Thus, a code which is superior or inferior at one (J/S) ratio will be assumed to be superior or inferior at all (J/S) ratios. A (J/S) ratio of 25 will be used to compare codes; this value is chosen primarily to illustrate a typical (J/S) ratio that might be required in an operational system.

Finally, since each modulation technique introduces a new parameter to the discussion, it is difficult to compare codes directly. Therefore, an example will be used to illustrate the relative effectiveness of each jamming code. This example consists of calculating the relative phase

50

error of each code at the same frequencies. Specifically, each code will be constrained to have 19 possible jamming frequencies. Again, the number 19 is chosen to illustrate a typical value that might be encountered in an operational system. A code with 19 jamming frequencies could cover a 200 Hz frequency band with a jamming component every 10 Hz.

Periodic Codes

The first modulation technique to be considered is the periodic pulse train illustrated in Figure 18. The code has a period of T and within each T second interval is a pulse
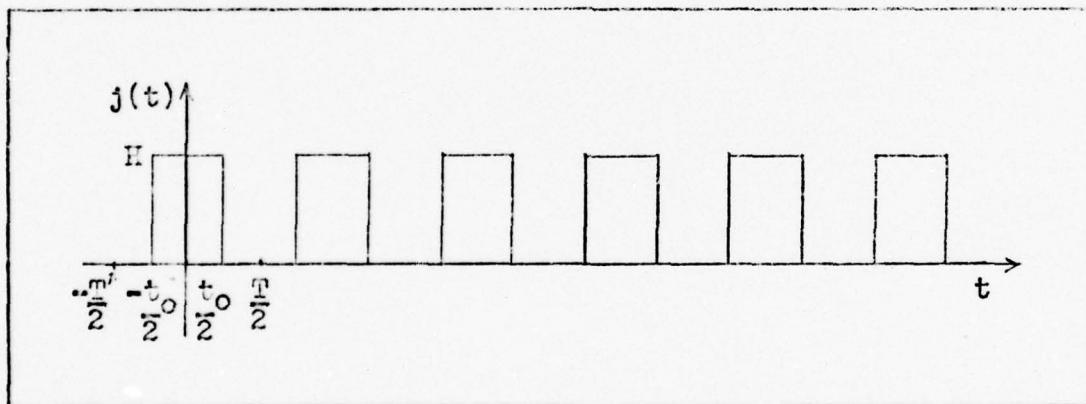
Figure 18. A Periodic Code

of duration t_o. It is assumed that T is some integer multiple of t_o. The ratio of t_o/T is the fraction of time that the code is on during any period, and as such will be called the duty-cycle of the code. The duty-cycle will play an important role in subsequent discussions.

As stated previously, the first step in evaluating this code is to find its frequency spectrum. Since $j(t)$ is periodic, it can be expanded in a Fourier series (Ref 8:32) of the following form

$$j(t) = A_o + \sum_{n=1}^{\infty} (A_n \cos\omega_n t + B_n \sin\omega_n t) \qquad (63)$$

where

$$A_o = \frac{1}{T} \int_{-\frac{T}{2}}^{\frac{T}{2}} j(t)dt \qquad (64)$$

$$A_n = \frac{2}{T} \int_{-\frac{T}{2}}^{\frac{T}{2}} j(t)\cos\omega_n t \, dt, \quad n = 1, 2, 3 \ldots \qquad (65)$$

$$B_n = \frac{2}{T} \int_{-\frac{T}{2}}^{\frac{T}{2}} j(t)\sin\omega_n t \, dt, \quad n = 1, 2, 3 \ldots \qquad (66)$$

and $\omega_n = \frac{2\pi n}{T}$. Eq (63) can be simplified by assuming that $j(t)$ is an even function; this assumption is valid, since, for purposes of this discussion, it matters little where the starting point of $j(t)$ is. Therefore, if $j(t)$ is assumed even then the term $[j(t) \sin\omega_n t]$ in Eq (66) is an odd function. Recall that the integral with symmetrical limits of an odd function is zero; therefore, the B_n's in Eq (66) and Eq (63) are zero. Thus, Eq (63) becomes

$$j(t) = A_o + \sum_{n=1}^{\infty} A_n \cos\omega_n t \qquad (67)$$

52

A plot of the magnitude of A_n versus ω_n will be the frequency spectrum of $j(t)$. Therefore, substituting for $j(t)$ in Eq (64) and Eq (65) results in

$$A_o = \frac{H}{T} \int_{-\frac{t_o}{2}}^{+\frac{t_o}{2}} dt = \frac{Ht_o}{T} \tag{68}$$

$$A_n = \frac{2}{T} \int_{-\frac{t_o}{2}}^{+\frac{t_o}{2}} H \cos\omega_n t \, dt \, , \quad n = 1, 2, 3 \ldots \tag{69}$$

Integrating Eq (69) yields

$$A_n = \frac{2Ht_o}{T} \frac{\sin\left(\frac{\omega_n t_o}{2}\right)}{\left(\frac{\omega_n t_o}{2}\right)} \, , \quad n = 1, 2, 3 \ldots \tag{70}$$

Eq (70) can be rewritten in the familiar $\sin x/x = \operatorname{sinc} x$ form as

$$A_n = \frac{2Ht_o}{T} \operatorname{sinc}\left(\frac{\omega_n t_o}{2}\right) \, , \quad n = 1, 2, 3 \ldots \tag{71}$$

If $t_o \ll T$, a plot of A_n versus frequency might look like the spectrum shown in Figure 19. From Figure 19 it is apparent that the frequency spectrum of a periodic code is a line spectrum with "zero-crossings" at the reciprocal of the pulse duration (t_o). The spacing of the frequency components is determined by the period (T) of the code, and the number of frequency components prior to the first zero-crossing is determined by the relationship T/t_o. That is,

53
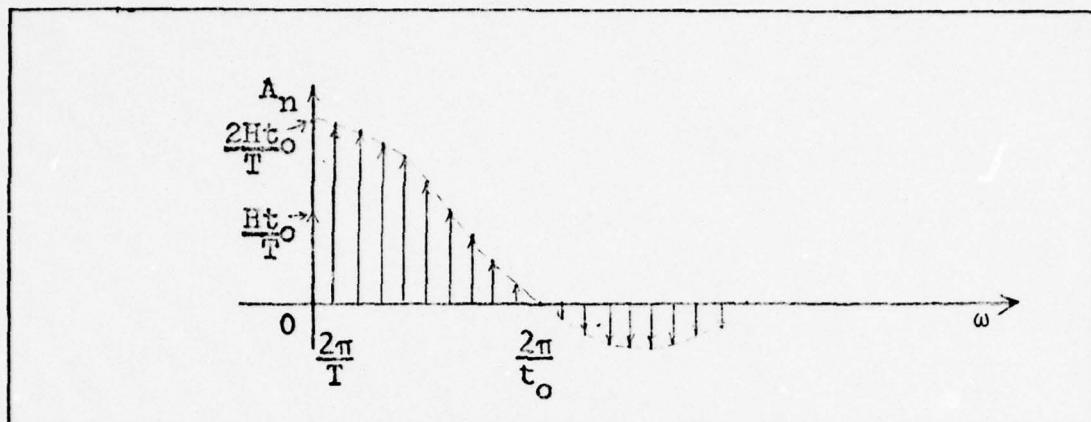
Figure 19. Frequency Spectrum of a Periodic Code

if T/t_o is some integer m, then there will be m-1 frequency components prior to the first zero-crossing. Recall that T/t_o is the reciprocal of the duty-cycle.

With reference to Figure 19, a general evaluation of periodic codes will be made. The requirement that a "good" jamming code spread its energy over a desired frequency band is met by a periodic code. Since most of the energy of a periodic code is in the frequency components prior to the first zero-crossing, the frequency spread of the code can be controlled by varying the signal width t_o. The requirement that a code have high AC content is again met by a periodic code. An examination of Figure 19 shows that the magnitude of the first few frequency components is nearly twice as large as the DC component.

As stated earlier in this chapter, an example will be used to illustrate the relative effectiveness of a periodic code. Recall that this example constrains the code to 19

54

possible jamming frequencies. Thus, it will be shown that a
periodic code containing 19 possible jamming frequencies
must have a duty-cycle (i.e., t_o/T) of 1/20. Since almost
all of the energy in the function sinc(x) is found in the
frequency components prior to the first zero-crossing, only
those components are considered as jamming frequencies.
Furthermore, it can be seen from Figure 19 that a value of
$t_o/T = 1/20$ fixes the number of sinusoidal components at 19
(not including the DC component). To complete the example,
the relative phase error, Θ_e, for each of the 19 frequency
components will be found.

In order to find Θ_e, the value of α (fraction of peak
power in a particular frequency component) and β (fraction of
jammer peak power in the DC component) must be determined.
The value of β can be found from Eq (68), which is rewritten
here in slightly different form

$$A_o = \beta H = \frac{H t_o}{T} \tag{72}$$

where A_o is the average or DC value of the code. Notice
that β is also determined by the duty-cycle of the code
(t_o/T). Therefore, for this example, it is easy to see that
$\beta = 1/20$.

An expression for α may be found by rewriting Eq (71)
as

$$A_n = \alpha H = H\left[\frac{2 t_o}{T} \ \mathrm{sinc}\left(\left|\frac{\omega_n t_o}{2}\right|\right)\right] \tag{73}$$

55

therefore,

$$\alpha = \frac{2t_o}{T} \, \text{sinc}\left(\frac{\omega_n t_o}{2}\right) \qquad (74)$$

The value of α for each of the 19 frequency components is found tabulated in Table I. Also shown tabulated in Table I is the phase error, θ_e, which was calculated using Eq (59).

Table I

Relative Phase Error for a Periodic Code
($\beta = .05$, $(J/S) = 25$)

Frequency Component	α	$\theta_e(^o)$	Frequency Component	α	$\theta_e(^o)$
1	.0996	33.60	11	.0572	18.53
2	.0984	33.14	12	.0505	16.29
3	.0963	32.34	13	.0436	14.02
4	.0935	31.29	14	.0363	11.80
5	.0900	30.00	15	.0300	9.59
6	.0858	28.47	16	.0234	7.47
7	.0810	26.74	17	.0170	5.42
8	.0757	24.87	18	.0109	3.47
9	.0699	22.85	19	.0052	1.66
10	.0637	20.73			

The results in Table I can be interpreted as follows. For example, if the tenth frequency component of the code, i.e., f = 10/T, is the component closest to the scan frequency of the reticle and thus is the component passed by the missile's filters, then a relative phase error of 20.73° will be induced in the missile's tracking system. However,

keep in mind that the phase errors presented in Table I
are to be used for code comparison purposes only, and are
not meant to predict absolute tracking errors.

Pseudorandom Codes

The next type of modulation technique to be considered
is called pseudorandom or pseudorandom noise (PN). A typical
pseudorandom waveform is shown in Figure 20. The parameter
t_o is called the digit width or more commonly the chip width
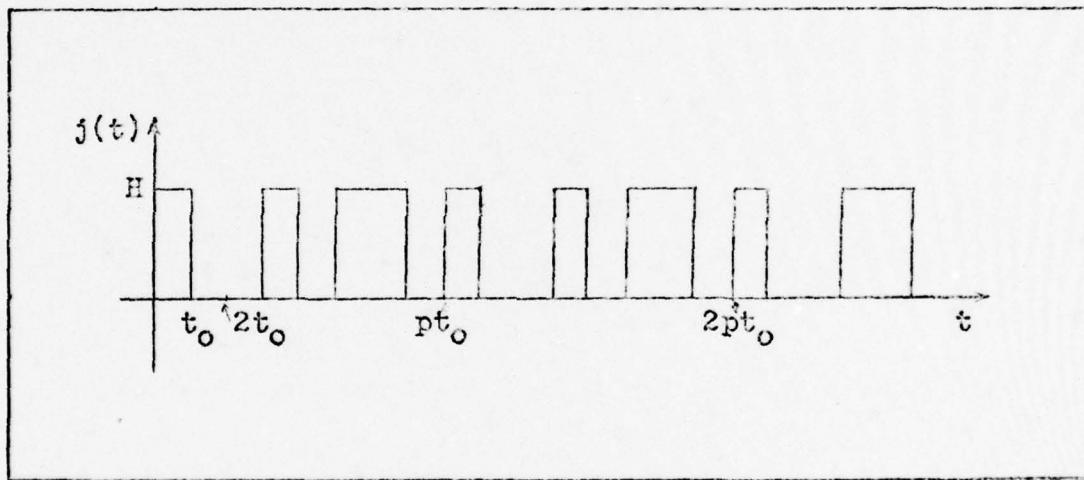

Figure 20. Typical Pseudorandom Code

of the code. The code repeats itself after p digits; there-
fore, p is the period of the code. A pseudorandom waveform
is a binary sequence, i.e., either +H or zero, and is easily
generated by using shift registers with predetermined feed-
back taps. The pseudorandom codes discussed in this section
are maximal length sequences. The above properties and

others of pseudorandom sequences are widely discussed in the literature (Ref 9; Ref 10; Ref 11:143-152).

The power spectral density of a pseudorandom waveform is given by (Ref 10:76)

$$S(\omega) = \frac{H^2}{4}\left[\frac{p+1}{p^2}\right]\left(\frac{\sin\left(\frac{\omega t_o}{2}\right)}{\frac{\omega t_o}{2}}\right)^2 \sum_{\substack{n=-\infty \\ n\neq 0}}^{+\infty} \delta\left(\omega - \frac{2\pi n}{p t_o}\right)$$
$$+ \frac{H^2}{4}\left[\frac{1}{p^2} + 1\right]\delta(\omega) \qquad (75)$$

where $S(\omega)$ is the power spectral density of the pseudorandom sequence. Eq (75) is a two-sided spectrum; to simplify later calculations, the one-sided power spectral density is written as

$$S(\omega) = \frac{H^2}{2}\left[\frac{p+1}{p^2}\right]\left(\frac{\sin\left(\frac{\omega t_o}{2}\right)}{\frac{\omega t_o}{2}}\right)^2 \sum_{n=1}^{+\infty} \delta\left(\omega - \frac{2\pi n}{p t_o}\right)$$
$$+ \frac{H^2}{4}\left[\frac{1}{p^2} + 1\right]\delta(\omega) \qquad (76)$$

In order to find the phase error, θ_e, due to a pseudo-random jammer, the frequency spectrum, $J(\omega)$, is needed. Recall that the power, P, in a sinusoid, $A \cos(\omega_n t)$, is given by

$$P = \frac{A^2}{2} \qquad (77)$$

Since Eq (76) gives the power of a pseudorandom waveform for each sinusoidal frequency component, the amplitude of each frequency component can be found using Eq (77). Specifically, to find the amplitude of a component in $J(\omega)$, the square root of two times the value of $S(\omega)$ at that frequency is taken. If this procedure is repeated for all frequencies in $S(\omega)$, an expression for $J(\omega)$ can be written as

$$J(\omega) = H \left[\frac{p+1}{p^2} \right]^{\frac{1}{2}} \text{sinc}\left(\frac{\omega t_o}{2} \right) \sum_{n=1}^{+\infty} \delta\left(\omega - \frac{2\pi n}{p t_o} \right)$$

$$+ \frac{H}{2} \left[\frac{1}{p} + 1 \right] \delta(\omega) \qquad (78)$$

It is clear from Eq (78) that the frequency spectrum of a pseudorandom code is also a line spectrum. The envelope of the line spectrum follows the function $\text{sinc}(x)$ with zero-crossings at $\omega = \frac{2\pi}{t_o}$. That is, the chip width t_o of the PN sequence determines the bandwidth of the code. Notice also that the frequency components of Eq (78) occur at intervals of $1/p t_o$. Thus, the number of possible jamming frequencies (components prior to the first zero-crossing) is determined by the length of the sequence, p. In other words, a pseudorandom code contains p-1 sinusoidal jamming frequencies.

As was done with periodic codes, an example will serve to illustrate the relative jamming effectiveness of a PN code. In this example the phase error, θ_e, for a PN code

59

containing 19 jamming frequencies will be computed. From
the foregoing paragraph, it is seen that a PN code containing
19 jamming frequencies must have a length of 20. Shown in
Table II is a tabulation of the phase errors for each of
these 19 frequencies. The values of α and β in Table II
were found from Eq (78) in a manner similar to that described
for periodic codes.

Table II

Relative Phase Error for a Pseudorandom Code
$(\beta = .525, (J/S) = 25)$

Frequency Component	α	$\theta_e(^{\circ})$	Frequency Component	α	$\theta_e(^{\circ})$
1	.2281	11.15	11	.1310	6.37
2	.2254	11.01	12	.1156	5.62
3	.2208	10.78	13	.1000	4.86
4	.2144	10.47	14	.0842	4.09
5	.2062	10.06	15	.0688	3.34
6	.1966	9.59	16	.0536	2.60
7	.1856	9.05	17	.0390	1.89
8	.1734	8.45	18	.0250	1.21
9	.1600	7.79	19	.0120	0.58
10	.1458	7.10			

A comparison of the phase errors in Table I and Table II
shows the pseudorandom code to be considerably inferior to
the periodic code at all 19 jamming frequencies. This is
because the average or DC component of the pseudorandom code
is large in comparison to the amplitude of its sinusoidal
components. It can be easily seen from Figure 20 that the

60

DC value of a pseudorandom code will be approximately $N/2$;
hence, a large portion of the code's total energy aids
the missile in tracking the target. Therefore, the results
of Table II reemphasizes the fact that an effective jamming
code must have a small DC component relative to the ampli-
tude of its AC components.

Random Binary Codes

A random binary code is one which every T seconds emits
one of two signals, either $s_1(t)$ or $s_2(t)$. Which signal to
emit during any T second interval is determined probabilis-
tically; that is, $s_1(t)$ is emitted with probability q and
$s_2(t)$ is emitted with probability $1-q$.

The power spectral density, $S(f)$, of such a modulation
scheme is given by the following expression (Ref 11:19)

$$S(f) = \frac{1}{T^2} \sum_{n=-\infty}^{+\infty} \left| q\, S_1\left(\frac{n}{T}\right) + (1-q)\, S_2\left(\frac{n}{T}\right) \right|^2 \delta\left(f - \frac{n}{T}\right)$$

$$+ \frac{1}{T} q(1-q) \left| S_1(f) - S_2(f) \right|^2 \qquad (79)$$

where $S_1(f)$ and $S_2(f)$ are the Fourier transforms of the
elementary signals $s_1(t)$ and $s_2(t)$. Notice that $S(f)$ is
composed of both a line spectrum and a continuous spectrum.
Thus, a random binary code is capable of producing both
sinusoidal and noise jamming.

In order to find the phase error due to such a random
binary jammer, the analysis must be handled in two parts.

61

The line spectrum will be used to find the phase error due to sinusoidal jamming and the continuous spectrum will be used to find the phase error due to the noise jamming.

The line frequency spectrum of the code, denoted as $J_L(f)$, can be found from the power spectral density, $S(f)$, in the manner described for pseudorandom codes. Thus, from Eq (79) an expression for $J_L(f)$ can be written as

$$J_L(f) = \frac{1}{T} \sum_{n=-\infty}^{+\infty} \left| q\, S_1\left(\frac{n}{T}\right) + (1-q)S_2\left(\frac{n}{T}\right) \right| \delta\left(f - \frac{n}{T}\right) \quad (80)$$

Given a particular $s_1(t)$ and $s_2(t)$, Eq (80) can be used to find the α and β factors needed in determining the phase error due to sinusoidal jamming, Θ_e.

As an example, assume that $s_\alpha(t)$ is a square pulse of height H and duration t_o, where $t_o \ll T$ and $t_o/T = m$ (where m is some integer). Furthermore, assume that $s_2(t) = 0$. Notice that $s_1(t)$ is the same as one period of the periodic code discussed earlier in this chapter; therefore, the Fourier transform obtained for the periodic code, given by Eq (71), can be used for $S_1(f)$. Thus, for this example, Eq (80) becomes

$$J_L(f) = \frac{Hqt_o}{T} \sum_{n=-\infty}^{+\infty} \text{sinc}\left(\frac{\pi n t_o}{T}\right) \delta\left(f - \frac{n}{T}\right) \quad (81)$$

Eq (31) is a two-sided frequency; however, in keeping with the convention of using one-sided spectrums, $J_L(f)$ is rewritten as

$$J_L(f) = \frac{2Hqt_o}{T} \sum_{n=1}^{+\infty} \text{sinc}\left(\frac{\pi n t_o}{T}\right) \delta\left(f - \frac{n}{T}\right) + \frac{Hqt_o}{T} \delta(f) \qquad (82)$$

Both α and β can be computed from Eq (82). For example, the DC component of $J_L(f)$ is

$$J_L(o) = \frac{Hqt_o}{T} \qquad (83)$$

therefore,

$$\beta = \frac{qt_o}{T} \qquad (84)$$

where q is the probability of $s_1(t)$ being sent. Similarly, α is found to be

$$\alpha_n = \frac{2qt_o}{T} \text{sinc}\left(\frac{\pi n t_o}{T}\right) \qquad (85)$$

where α_n denotes α for the nth harmonic.

The relative jamming effectiveness of a random binary code will be compared against that of a periodic and pseudo-random code by means of an example. In keeping with the previous example, the random binary code is assumed to have 19 different jamming frequencies; thus, from Eq (85) it can be seen that $t_o/T = 1/20$. Furthermore, to simplify the calculations, assume $s_1(t)$ and $s_2(t)$ are equally likely or

63

$q = \frac{1}{2}$. A tabulation of the phase error, θ_e, for each of the 19 possible sinusoidal jamming frequencies is shown in Table III.

Table III

Relative Phase Error for Random Binary Code
(sinusoidal jamming only, $\beta = .025$, $(J/S) = 25$)

Frequency Component	α	$\theta_e(^o)$	Frequency Component	α	$\theta_e(^o)$
1	.0498	22.52	11	.0286	12.71
2	.0492	22.24	12	.0253	11.22
3	.0482	21.76	13	.0218	9.65
4	.0468	21.10	14	.0184	8.14
5	.0450	20.25	15	.0150	6.63
6	.0429	19.27	16	.0117	5.16
7	.0405	18.15	17	.0085	3.75
8	.0379	16.95	18	.0055	2.42
9	.0350	15.62	19	.0026	1.15
10	.0319	14.20			

A comparison of Table III with Tables I and II shows the random binary code to lie almost exactly between the periodic code and the pseudorandom code in relative jamming effectiveness. However, keep in mind that Table III contains only the phase error contributed by the line spectrum of the random binary code. The total phase error generated by a random binary code will also contain a contribution from the continuous spectrum.

64

The phase error induced by noise jamming, i.e., a
continuous frequency spectrum, can be computed from Eq (61)
which is rewritten here for convenience

$$\Theta_n \approx \left[\frac{NB_L}{A_d^2}\right]^{\frac{1}{2}} \tag{61}$$

where Θ_n is the phase error due to noise jamming.

An example will serve to illustrate the effect of noise
jamming on total system phase error. Suppose that the
signal-to-noise ratio, (A_d^2/N), is 1000 and that the loop band-
width, B_L, is 10 Hz. From Figure 16 it can be seen that
$\Theta_N \approx 6^{\circ}$; thus, the total system phase error, Θ_T, is the sum
of the Θ_e's shown in Table III and $\Theta_N = 6^{\circ}$. Therefore, the
contribution of Θ_N in this example makes the total phase
error for a random binary code almost as great as that of
the periodic code and considerably better than the PN code.

The reader should keep in mind that the foregoing
discussion of the phase error resulting from noise jamming
is intended as a crude estimate only. However, since
Figure 16 indicates that noise jamming is a potential source
of large jamming errors, it is recommended that a more com-
plete model of noise jamming be developed.

Other Modulation Techniques

The modulation techniques presented in this chapter
are by no means the only possible jamming codes available;
they were chosen because they represent three distinct types

65

of codes. Indeed, variations on the techniques presented herein can lead to a number of possible jamming schemes. For example, variations on random binary codes alone include: codes with Gaussian or cosine pulses instead of square pulses, codes with more than two signals, codes which delay signals from period to period, codes which are modulated by sinusoids or other codes. The performance of these codes and others could be evaluated using the techniques described in this thesis.

VI. Conclusions and Recommendations

This chapter will present some basic conclusions from the previous five chapters and several recommendations for further study will be given.

Conclusions

The major conclusions of this study are these:

1. The tracking performance of an AM, rotating-reticle IR system can be degraded by a sinusoidally-modulated IR source operating at the scan frequency of the reticle.

2. To permit jamming against reticle-based IR systems of varying or unknown scan rates, modulation techniques can be developed which allow jamming over a range of possible scan frequencies. Three such techniques--periodic, psuedo-random, and random binary--were discussed in this thesis.

3. Prospective jamming modulation techniques can be evaluated for relative jamming effectiveness using procedures developed in Chapter IV of this thesis.

4. Of the three modulation techniques presented, it appears that periodic and random binary codes are better suited to IR jamming applications than are pseudorandom codes.

5. The effectiveness of a jamming system will depend not only on the modulation technique employed, but also on the availability of IR sources with large peak powers.

Recommendations

The major suggestions for further study are these:

1. A study is recommended to determine if the results presented herein for an AM, rotating-reticle system can be extended to other types of reticle systems, such as FM, stationary-reticle systems.

2. A first-cut attempt was made to model a code with a continuous frequency spectrum as an additive noise source in the electrical network of an IR system. Further study is needed to test the validity of this model, and if the model is valid, further study is needed to determine the full potential, if any, of noise jamming.

3. The jammer model presented in this thesis was assumed to have an optimal phase angle with respect to the reticle system. In a simulated or operational system this would be an unrealistic assumption; therefore, further study is needed to resolve this phase reference issue.

4. As is the case with any theoretical undertaking, its true worth can only be ascertained after empirical evidence has collaborated its findings. Therefore, a physical simulation using the techniques described in this report is recommended.

Bibliography

1. Biberman, Lucien M. *Reticles in Electro-Optical Devices.*
   London: Pergamon Press, 1966.

2. Hudson, R. D. *Infrared System Engineering.* New York:
   John Wiley & Sons, 1969.

3. Ulrich, J. P., *et al.* *Analysis of Reticle Systems.*
   Willow Run Laboratory TR 6054-2-T. Ann Arbor, Michigan:
   The University of Michigan, October 1965. AD 472560.

4. Alward, James L. *Spatial Frequency Filtering.* Willow
   Run Laboratory TR 2389-87-T. Ann Arbor, Michigan: The
   University of Michigan, December 1965. AD 480352.

5. Aroyan, George F. "The Technique of Spatial Filtering."
   Proceedings of the Institute of Radio Engineers, 47:
   1561-1568 (September 1959).

6. Papoulis, Athanasios. *Fourier Integral and Its Appli-
   cations.* New York: McGraw-Hill Book Company, 1962.

7. Ziemer, R. E. and Tranter, W. H. *Principles of
   Communication.* Boston: Houghton Mifflin Company, 1976.

8. Schwartz, Mischa. *Information Transmission, Modulation,
   and Noise.* New York: McGraw-Hill Book Company, 1970.

9. Dixon, R. C. *Spread Spectrum Systems.* New York: John
   Wiley & Sons, 1976.

10. Golomb, Solomon W. *Digital Communications with Space
    Applications.* New Jersey: Prentice-Hall, Inc., 1964.

11. Lindsey, W. C. and Simon, M. K. *Telecommunication
    System Engineering.* New Jersey: Prentice-Hall, Inc.,
    1973.

12. Viterbi, A. J. *Principles of Coherent Communication.*
    New York: McGraw-Hill Book Company, 1966.

Vita

Carl F. Moore was born 28 September 1948 in Portsmouth, Virginia. He graduated from high school in Jacksonville, Arkansas, in 1966. He graduated from the University of Arkansas in 1970 with a Bachelor of Science in Electrical Engineering degree. Also in 1970, he was commissioned in the USAF by way of OTS. After graduating from OTS, he attended Undergraduate Pilot Training at Craig AFB, Alabama. He graduated from UPT in 1971. From 1972 until he entered AFIT in 1976, he served as a C-141 pilot at McChord AFB, Washington.

    Permanent address: Oakwood Mobile Home Park
                        Jacksonville, Arkansas   72076

REPORT DOCUMENTATION PAGE	READ INSTRUCTIONS BEFORE COMPLETING FORM

1. REPORT NUMBER	2. GOVT ACCESSION NO.	3. RECIPIENT'S CATALOG NUMBER
AFIT/GE/EE/77-30		

4. TITLE (and Subtitle)	5. TYPE OF REPORT & PERIOD COVERED
MODULATION TECHNIQUES FOR DEFEATING PASSIVE RETICLE-BASED INFRARED SYSTEMS	MS Thesis
	6. PERFORMING ORG. REPORT NUMBER

7. AUTHOR(s)	8. CONTRACT OR GRANT NUMBER(s)
Carl F. Moore Capt.	

9. PERFORMING ORGANIZATION NAME AND ADDRESS	10. PROGRAM ELEMENT, PROJECT, TASK AREA & WORK UNIT NUMBERS
Air Force Institute of Technology (AFIT-EN) Wright-Patterson AFB, Ohio 45433	

11. CONTROLLING OFFICE NAME AND ADDRESS	12. REPORT DATE
Electro-Optical Warfare Branch (AFAL/WRW) Air Force Avionics Laboratory Wright-Patterson AFB, Ohio 45433	Dec, 1977
	13. NUMBER OF PAGES
	69

14. MONITORING AGENCY NAME & ADDRESS(if different from Controlling Office)	15. SECURITY CLASS. (of this report)
	Unclassified
	15a. DECLASSIFICATION/DOWNGRADING SCHEDULE

16. DISTRIBUTION STATEMENT (of this Report)

Approved for public release; distribution unlimited

17. DISTRIBUTION STATEMENT (of the abstract entered in Block 20, if different from Report)

18. SUPPLEMENTARY NOTES

Approved for public release; IAW AFR 190-17

JERRAL F. GUESS, Captain, USAF
Director of Information

19. KEY WORDS (Continue on reverse side if necessary and identify by block number)

optical countermeasures
infrared countermeasures
reticles

20. ABSTRACT (Continue on reverse side if necessary and identify by block number)

A mathematical analysis of an amplitude-modulated (AM), rotating-reticle, infrared (IR) system was conducted. The purpose of this analysis was to construct a theoretical model of the above IR system, so that methods of defeating or jamming such a system could be developed and studied. Using this model, two types of jamming- sinusoidal and noise- were shown to be effective against the AM-reticle system. Three IR modulation techniques-periodic, pseudorandom, and random binary- which produce these types of

DD FORM 1473 EDITION OF 1 NOV 65 IS OBSOLETE

20. jamming were presented and analyzed.